JOURNAL OF RESEARCH of the National Bureau of Standards
Vol. 88, No. 6, November-December 1983

CONTENTS

Library of Congress Catalog Card Number: 63-37059

**For sale by the Superintendent of Documents, U.S. Government Printing Office
Washington, DC 20402
Single copy price $5.50 Domestic; $6.90 Foreign.
Subscription price: $18.00 a year; $22.50 foreign mailing.
UNITED STATES GOVERNMENT PRINTING OFFICE, WASHINGTON: 1983**

JOURNAL OF RESEARCH of the National Bureau of Standards
Vol. 88, No. 6, November-December 1983

A Polystyrene-Water Calorimeter

Steve R. Domen

National Bureau of Standards, Washington, DC 20234

Accepted: July 15, 1983

The paper describes a new type of calorimeter that can be quickly put into operation for determining absorbed dose at a point in polystyrene. It also describes a unique method of decreasing drifts in electrical signals caused by temperature gradients. Two calibrated thermistors were placed close together between sandwiched polystyrene discs that were immersed in water. The assembly was irradiated with gamma rays from a cobalt-60 source. The dose rate was about 14 mGy/s and exposure times were about 100 s. The standard deviation for a daily set of measurements was about 0.7%. A zero heat defect for polystyrene was assumed. A calculation converted the measurements to absorbed dose in water. The dose in water determined in this way, and with a graphite calorimeter, is 3–4% lower than that measured in an all-water calorimeter previously reported. Drifts in electrical signals are eliminated by a resistance-capacitance circuit placed across a Wheatstone bridge. The rate of potential change across the bridge (caused by the circuit) is adjusted to have an opposite effect to the drifts in electrical signals produced by temperature gradients within the calorimeter. The method can be applied to other calorimeters.

Key words: absorbed dose; calorimeter; heat defect; polystyrene; temperature drifts; thermistor; water.

1. Introduction

One purpose of this paper is to report on an investigation of a calorimeter for measuring absorbed dose[1] *at a point in polystyrene* and converting the results to also give absorbed dose in water. Another purpose is to describe a method of balancing drifts in electrical signals caused by temperature gradients. In general, the method can be applied to other calorimeters.

The calorimeter and the method of drift balance have been briefly described in previous publications [1,2].[2] In the present paper, the calorimeter (particularly) is described in detail.

Because the standard absorbing material is water [3], recent investigative studies of a calorimeter for measuring absorbed dose *at a point in water* were undertaken and reported [4,5]. It was pointed out [5] that the first major effort in the development of this type of calorimeter (in overcoming the physical problems of accurately and efficiently measuring a temperature rise at a point in water) was successful—but that the second major effort still remained, that is, to determine the existence of and corrections for heat defects in irradiated water (heat defect is the energy absorbed or released in induced radiation chemical reactions, being positive or negative depending, respectively, on whether an endothermic or exothermic reaction takes place). Under cobalt-60 irradiation, the apparently measured absorbed dose rate in distilled water is 3.5% higher [5] than results obtained with a graphite calorimeter [6], the results being converted to apply to water [7]. Nearly the same result, 3.8% (derived from comparisons with ionization measurements), was reported [8] as a result of measurements made in a copy of the water calorimeter irradiated with cobalt-60 gamma rays and with photon beams up to a maximum energy of 25 MeV; but for the case with electrons from 13 to 20 MeV, the results with the water calorimeter were 1% lower than those derived from ionization measure-

About the Author: Steve R. Domen is a physicist in NBS' Radiation Physics Division.

[1] Absorbed dose is the mean energy per unit mass imparted to matter by ionizing radiation. The SI unit of absorbed dose is the gray (symbol Gy). 1 Gy = 1 J/kg (= 100 rad).

[2] Figures in brackets indicate literature references at the end of this paper.

ments. This lower result does not appear to be in agreement with measurements in another copy of the calorimeter irradiated with 17 and 22 MeV electrons [9], nor with what would be expected from theoretical calculations [10,11]. Reference [11] indicates that calorimetric results should be the same for photons as well as for electrons, assuming that the initial conditions of the water are effectively the same.

Comparison of results with other types of calorimeters would aid in the possible realization of an accurate and efficient instrument for use under widely different irradiation conditions. Such calorimeters should be constructed of materials having absorption properties close to that of water and having a negligible or known heat defect. Polystyrene is such a possible material. By using the techniques described in this paper, other materials can be used to compare their heat defects as a function of accumulated dose—to investigate them for potential calorimetric use.

Reported results [12] indicate a $0.0\pm0.8\%$ heat defect in a polystyrene sample irradiated with cobalt-60 gamma rays, after a pre-irradiation of about 2 kGy. Within experimental error, no heat defect was observed with fast neutrons [13]. Other reported results [14] indicate that a polystyrene sample (from a different manufacturer) irradiated with 30-kV x-rays gave only borderline evidence of a heat defect, $(0.67\pm0.94)\%$ standard deviation, a constant result as a function of accumulated absorbed dose. A heat defect of 0.1% was reported for polystyrene irradiated with 1.7 MeV protons ([3], p. 14). Although these are limited irradiation conditions, the results suggested the construction and investigation of an absorbed dose calorimeter in which measurements are made directly in polystyrene and the comparison of this calorimeter with the water and graphite calorimeters under a wide range of conditions.

The present paper describes and reports results of investigations with a polystyrene-water calorimeter irradiated with gamma rays from a cobalt-60 source. This combination of solid and liquid materials makes possible an efficient instrument that can be brought quickly into operation and balanced (in contrast to one with a large solid polystyrene cylinder and no means of controlling temperature drifts [15]). Advantage is taken of the mobility of water in quickly bringing it and a relatively thin polystyrene disc close to a uniform operating temperature.

Rapid control of objectionably large drifts (caused, for example, by small remaining temperature differences between the discs and water, or by successive runs with collimated beams of low-energy electrons) is a vital feature that a calorimeter must have to encourage its construction and use. In the water calorimeter previously reported, the drifts were essentially instantly controlled by making a small change in electrical power dissipated in the water [5]. In the presently described calorimeter, the drifts are also rapidly decreased by changing the internal temperature gradients in addition to applying another simple technique. This technique consists of merely changing a charging potential applied to a resistance-capacitance (RC) circuit placed across a Wheatstone bridge, to produce a changing potential across the bridge that has an effect opposite to that caused by remaining small temperature gradients.

This paper describes the new features and operation of the polystyrene-water calorimeter in detail. However, many details are not described or are only briefly described because the only physical difference between the present calorimeter and the water calorimeter is the detector that is used. Construction features, the bridge circuit, calorimeter setup, thermistor sensitivity measurements, and corrections for thermistor power dissipations have been detailed [5]. The present paper, too, is written in detail to aid those in particular who may want to construct the calorimeter and understand its design and behavior.

2. Measurement Theory

Advantage was taken of the low thermal diffusivity of polystyrene and water, which retard a temperature change at a point of measurement. Two bead thermistors were positioned close together between sandwiched polystyrene discs immersed in water. The thermistors formed opposite arms of a Wheatstone bridge to double the sensitivity in comparison with a one-thermistor bridge.[3] The absorbed dose is

$$D=(1/2)(\Delta R/R)(\bar{S}^{-1})(c), \qquad (1)$$

where D is the absorbed dose,

(1/2) is the result of using two thermistors to measure a temperature,

$\Delta R/R$ is the fractional change in the Wheatstone bridge balancing resistor,

$\bar{S}$ is the mean fractional change in resistance of the thermistors per unit temperature rise, and

c is the specific heat capacity of polystyrene.

[3] The sensitivity could be doubled with a one-thermistor bridge, by doubling the potential applied across the bridge. This would quadruple the thermistor power dissipation. Reference [5] points out reasons for maintaining as low a power level as possible.

If c is in J/(g·K), D is in kGy. The product $(1/2)(\Delta R/R)(\bar{S}^{-1})$ is the temperature rise. The sensitivity, $\bar{S}$, was determined to an uncertainty of about 0.1%.

The sensitivity is nominally 4% per degree and decreases by seven parts per thousand per degree increase at room temperature. The value of c increases by four parts per thousand per degree at room temperature. Calculated changes in $\bar{S}$ and c were determined by use of a probe mounted inside the calorimeter and connected to an instrument that displayed temperature with a resolution of 0.01 K.

The value of c used in this investigation, at an operating temperature of 22.5 °C, was 1.203 J/(g·K). This value was calculated from an equation [16]:

$$c=(104.15)^{-1}(7.7551\cdot10^{5}\ T^{-2}+0.53447T-41.58)$$

J/(g·K), (2)

where T is the absolute temperature. One mole of polystyrene = 104.15 g.

Equation (2) was fitted to results of specific heat capacity measurements (of various samples of amorphous polystyrene which had a density of 1.05 g/cm^3) determined by various investigators, from 200 K to 360 K. The reported rms deviation is 0.5%. Only selective results were used which were judged to meet satisfactory standards based on experimental technique, error limits, and accuracy of representation of the data.

Although a calculated value appears to be a reasonable result to use in this investigation, attempts are being made to determine the specific heat of samples (from which the detector was made) to an accuracy and precision within a few tenths of 1%. Any further results or changes will be reported in a future publication.

3. The Calorimeter

Figure 1 shows some features of the calorimeter. Two 0.25 mm diameter bead thermistors are embedded near the central plane of two sandwiched discs of clear polystyrene. The central plane is near a 5/cm^2 depth in once-distilled water that is partially electrically conductive. The discs are fastened to three acrylic rods secured to the bottom of a 30 cm cube water container constructed of acrylic material (mounting the rods on a vertical wall, and providing an entrance window, permits measurements with

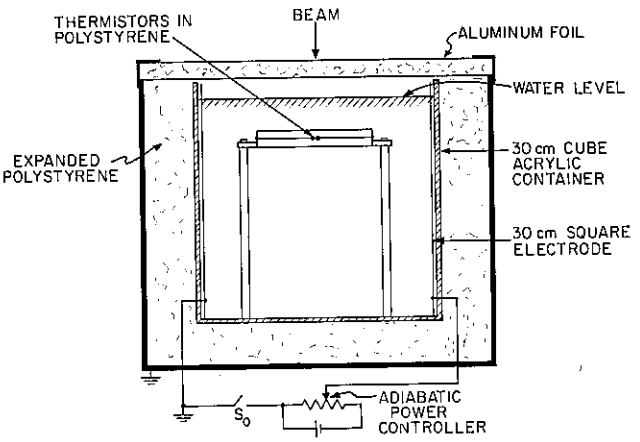

Figure 1–Essential features of the absorbed dose polystyrene-water calorimeter. The "adiabatic" power controller permits a potential to be applied across the electrodes so that in the vicinity of the discs the rate of temperature rise of the water, as a result of electrical power and beam irradiation, is as nearly as possible the same as that of the discs.

horizontal beams). Two electrodes (30 cm square stainless steel) for "adiabatic" operation are secured against opposite walls inside the container (in the water calorimeter they were the drift control electrodes [5]). The potential supply consists of a series-parallel arrangement of four 67.5 V drycell batteries which provide 135 V across a 10-turn 50-kΩ helipot. Closing switch S_0 causes heating of the water. Measurements of potential across the electrodes and current through the stagnant water permit the determination of the rate of temperature rise of the entire water bath. The potential, V, is predetermined so that the rate of temperature rise of the water in the vicinity of the discs (as a result of electrical power and beam irradiation) produces as nearly as possible the same rate of temperature rise as do the polystyrene discs heated directly with broad beam irradiation. The electrical resistance of the water, usually in the range of 10–25 kΩ, decreased during a daily set of measurements by about a factor of 2. This increased the drifts but these could be reduced by making small changes in the adiabatic power controller.

The approximate potential across the electrodes is pre-determined as follows: The rate of temperature rise of the polystyrene can be calculated from the absorbed dose rate and the specific heat of polystyrene, or it can be determined from the measured rate of fractional resistance change of the known thermistor sensitivities. Considering that the specific heat of water is 3.5 times greater than that of polystyrene, and that the absorbed dose rate and heat

defect in water are each approximately 3% greater, the rate of temperature rise in polystyrene irradiated with cobalt-60 gamma rays is approximately 3.3 times greater than that of water. The purpose of the electrical heating of the water is to make up the difference. Before an irradiation run (and particularly before the first run), an arbitrary potential, V_1, produced a current I_1. These measured values permitted a calculation of the electrical resistance of the water. The values V_1 and I_1 also permitted (as a first approximation) the calculation of the approximate potential, V, to accomplish adiabatic operation. Observations of the afterdrifts showed, however, that this value was too high by approximately 10%. The reason for this is that the derivation of V assumed a uniform current density throughout the water where in reality the current lines must necessarily be forced to flow around the discs.[4] This causes a greater current density and thus a greater heating effect in the vicinity of their flat surfaces. A reasonably accurate formula was found to be

$$V \cong 0.9\sqrt{\dot{D}V_1/I_1}, \qquad (3)$$

where $\dot{D}$ is the absorbed dose rate in Gy/min. In practice, observations of the drifts will indicate when the potential, V, needs to be adjusted.

4. The Detector

Figure 2 shows some details of the detector. Each thermistor, positioned 1 mm from the disc axis, is embedded just underneath each inner surface. Each disc is 10 mm thick and 152 mm in diameter. Mainly to avoid damage to the wiring during assembly (and because of heat transfer considerations), the discs are separated by three 0.3 mm thick paper spacers (6 mm in diameter) equally spaced near the disc circumference. Silicone rubber is applied around the discs' central plane to provide a watertight seal. The signal leads are connected to a waterproofed electrical socket fastened near the circumference of the lower disc. A small hole drilled along the axis of the socket permits enclosed air between the discs to vary with changes in atmospheric pressure.

It will be pointed out later that good mechanical and thermal anchoring (other than through air)

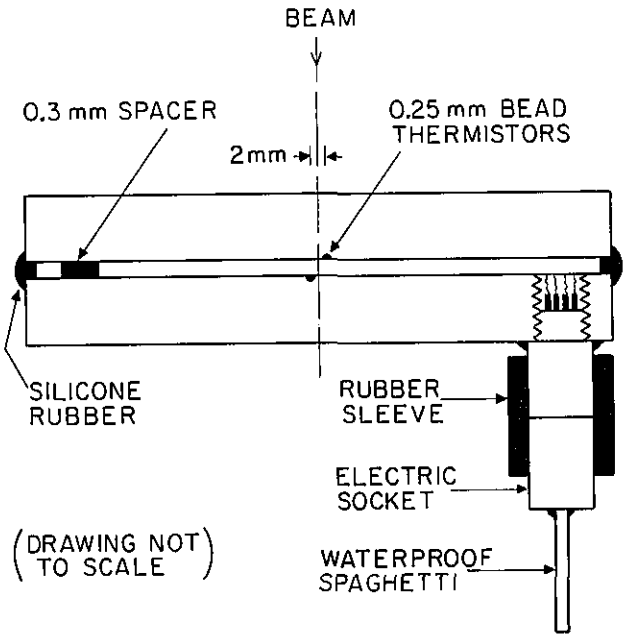

Figure 2–Constructional details of the detector. Each of the two polystyrene discs is 10 mm thick and 152 mm in diameter.

between the discs and thermistors (including the wires leading from them, for a length of at least 1 cm) seems to result in important and desirable detector behaviors. Figure 3 shows the wiring configuration. A compass was used to scribe grooves *slightly larger* than the embedded wires. Each thermistor bead was commercially fused around two 25 μm diameter wires (90% platinum, 10% iridium) which are soldered to 25 μm diameter copper wires (the copper wires have a higher thermal conductivity by a factor of 12). *The thermistors and the 1 cm lengths of Pt-Ir wires are totally embedded in epoxy resin.* The copper wires are partially embedded in silicone rubber (which aided in the initial layout), and the remainder is entirely embedded in epoxy resin. The embedments were done with the aid of a microscope which also aided in removing minute amounts of embedding material outside the grooves. This precaution (and considering that their specific heat capacities are not largely different from that of polystyrene) made the irradiation thermal effects of those remaining materials negligible. The thermal effect of irradiating the small amounts of different materials (other than polystyrene) composing the wires and thermistors is negligible, *<0.01% within a few seconds after irradiation [5].*

The purpose of the shown configuration (in preference to directing the wires directly to the socket) is to decrease possible conductive effects along the wires (caused by variations in radial dose rates)

[4] If the chosen discs are electrically conductive (such as A-150 plastic [17] or graphite which has a reported heat defect near zero), then they must be electrically insulated from the water. Reference [18] reports an endothermic heat defect of about 4% for A-150 plastic irradiated under different conditions.

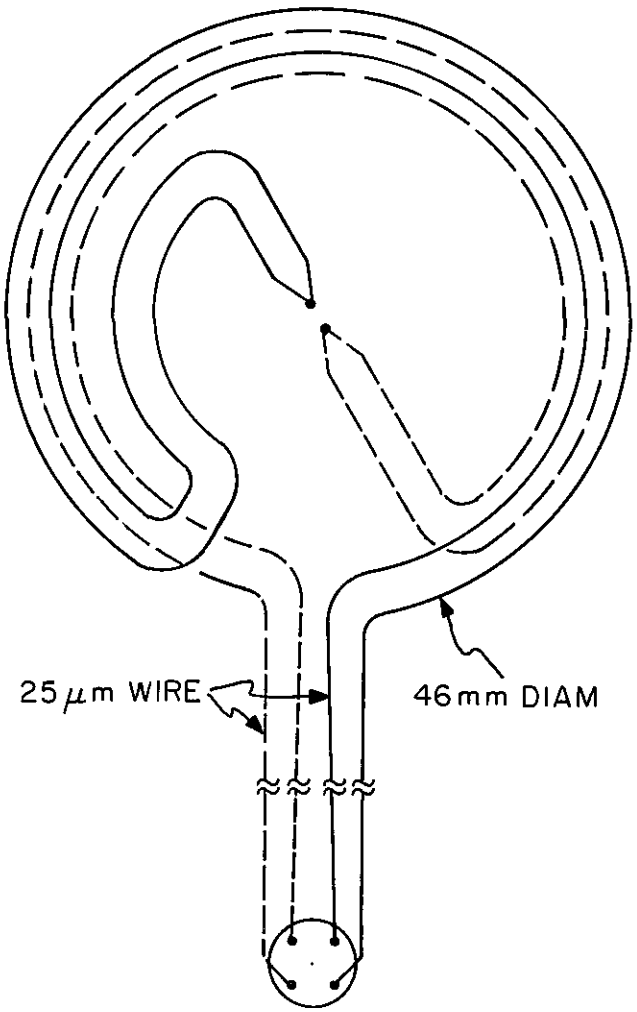

Figure 3–Wiring configuration of the detector.

which would tend to affect a temperature measurement. Because the longer lengths increase the resistance of the wires, their resistances are calculated to correct for their effects.

The measured density of the polystyrene discs was 1.050 g/cm^3. The discs' electron density (electrons per unit volume) is only 2% greater than that of water.

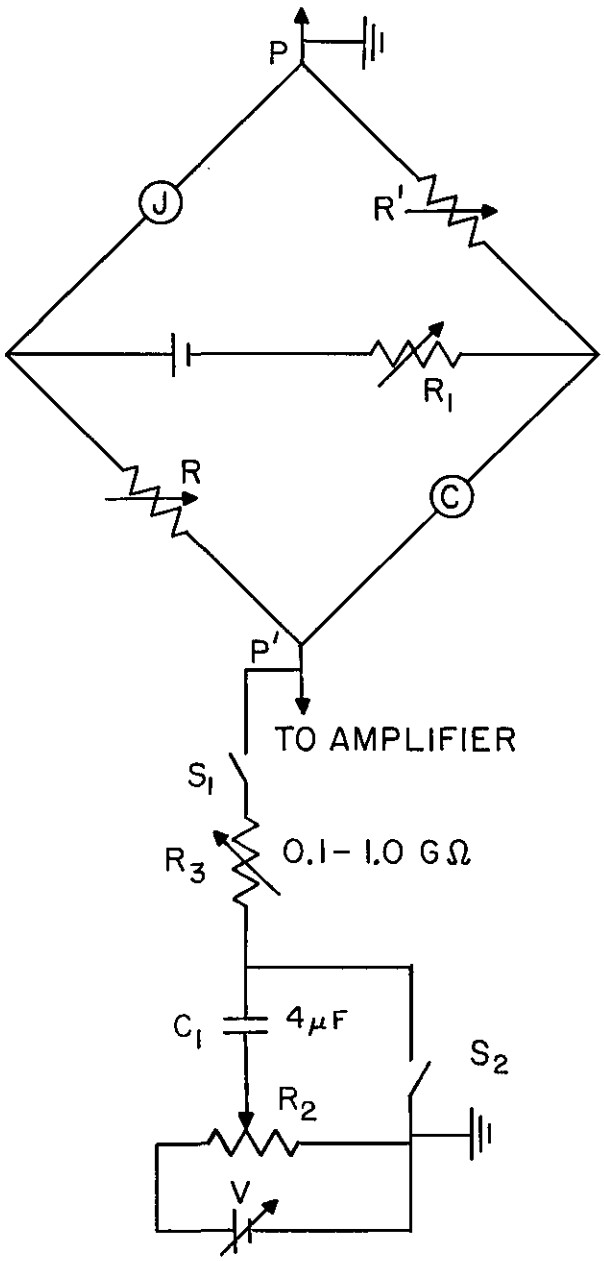

Figure 4–Wheatstone bridge circuit and signal drift balancer.

5. The Wheatstone Bridge

The upper part of figure 4 shows the simplified dc Wheatstone bridge circuit containing two thermistors. The circuit is used for determining both the fractional resistance change ($\Delta R/R$) in the balancing resistor (R) and the fractional change in thermistor resistance per degree temperature rise (S) of each thermistor, C and J—for use in eq (1). A selector switch permits measurements in the shown (C+J) mode, or in the C or J mode. Each arm of the bridge has a nominal resistance of 3 kΩ. The dc output of the bridge was connected to a nanovolt null detector that consisted of a chopper, ac amplifier, and demodulator system followed by a dc amplifier.

6. The Drift Balancer

The new design feature is the RC-circuit, shown in the lower part of figure 4. Switch S_1 permits the

circuit to be either connected across or disconnected from the bridge and amplifier. The amplifier normally has a small input resistance of about 300 kΩ compared to at least 0.1 GΩ of the RC-circuit. Its use and further details of the electrical signal drift balancer are described below.

7. Thermistor Sensitivity Measurements

The thermistor resistance value (r) at a given absolute temperature (T) is given by the well-known empirical expression:

$$r=r_0 e^{\beta(1/T-1/T_0)}, \tag{4}$$

where r_0 is the resistance at temperature T_0 and β is the "material constant."

The sensitivity of a thermistor (S) is defined as $(1/r)(dr/dT)$, which gives

$$S=-\beta/T^2. \tag{5}$$

Equation (4) can be reduced to linear form:

$$y=\beta x+\theta, \tag{6}$$

where $y=\ln r$, $x=1/T$, and $\theta=\ln r_0-\beta/T_0$, a constant. Least-squares fits of the data are applied to eq (6).

Resistance measurements were made in a temperature range of 16–28 °C, in steps of 2 degrees. A crystal thermometer (1 mK resolution) measured the temperature of the surrounding agitated water. When necessary, the temperatures were maintained within several millikelvin by adding ice water or by momentarily supplying 400 W of electrical power to immersion heaters (not shown in fig. 1).

The relatively small thickness (10 mm) of each sandwiched disc results in a reasonably short time for the thermistors to reach their ultimate temperature change. This is illustrated in figure 5. It shows the result of calculations from the use of theoretical values tabulated [19,20] combined with a thermal diffusivity of 12.4×10^{-4} cm^2/s determined from a table of recommended values for polystyrene [21], at the calorimeter operating temperature (for water it is 14.4×10^{-4} cm^2/s).

Consider that the entire system is at initial temperature T_i and that the agitated water is suddenly raised (or lowered) in temperature to T_f. The curve shows the amount of temperature change (in percent of the ultimate temperature change) of the thermistors as a function of time. At 26 and 39 minutes the thermistors theoretically reach, respectively, 99 and 99.9% of their total temperature change. (Figure 5 applies to any pair of sandwiched polystyrene discs each of thickness t cm, when the shown numerical values of the abscissas are multiplied by t^2.) However, at 30–35 min (in practice) the bridge output indicated that further resistance (temperature) changes were insignificant. The resistances were then determined from the known resistance values of R and R' and from measured potentials across each bridge arm.

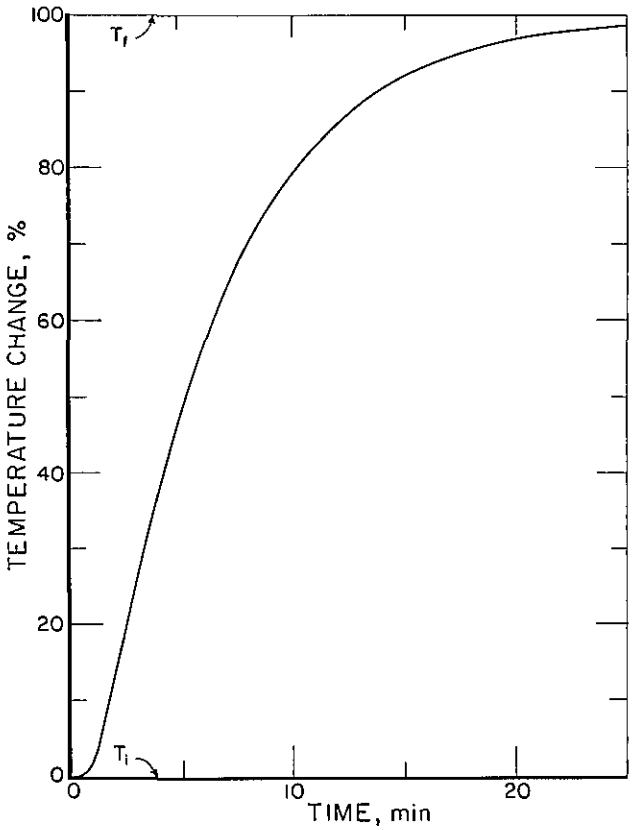

Figure 5–Temperature equilibration at the central plane of the sandwiched polystyrene discs, each 10 mm thick.

The results are shown in table 1. The first set of measurements was made before the calorimeter underwent radiation. Two months later a second set of measurements was made after the detector had received 1.33 kGy of absorbed dose. The results show

Table 1. Measured values of the "material constant," β

Accumulated dose (kGy)	β_C (K)	β_J (K)
0	3134.1	3178.6
1.33	3137.2	3177.6
	3135.7	3178.1

insignificant changes. A mean value, $\bar{\beta}$, of 3157 K was used for the (C+J) mode indicated in figure 4.

8. Calorimeter Setup

In order to compare results, the polystyrene-water calorimeter was irradiated under conditions essentially identical to those of the graphite and water calorimeters. Irradiations were made with the same cobalt-60 unit collimated to give the same-sized broad beam. Optical sighting and micrometer measurements were used to accurately position the central planes of the sensing units near 1 m from the source and at a mass depth near 5 g/cm^2.

9. Drift Balance

Reduction of temperature gradients which cause drifts first requires elimination of large drifts (after water is introduced in the calorimeter) and then reduction and stabilization of subsequent small drifts observed at high amplification.

The calorimeter was most stable when it was made uniform in temperature at the room temperature regulated near 22.5 °C. The introduced water was about 1 degree cooler. This caused cooling of the polystyrene discs during the calorimeter setup. The water was then agitated with a gas and raised to room temperature by use of the immersion heaters. The heaters were then turned off, but the agitation continued. The output of the Wheatstone bridge indicated the general thermistor response shown in figure 5. At about 30–35 minutes the agitation was turned off. Irradiation measurements were made when the water was stagnant (tests showed that this condition permitted much better reduction and control of drifts than when the water was agitated and raised in temperature during a measurement).

In theory, it would seem that prolonged agitation would result in insignificant temperature drifts. In practice, subsequent drifts observed at high amplification should not be expected to be zero, to remain constant, or to be small because they can change as a result of a number of internal and/or external causes. Significant drifts were usually observed after prolonged agitation. This could have been caused by the temperature of the incoming agitating gas and/or as a result of heat exchange with the outside of the container which may have resulted in a small temperature difference between the water and discs. As a result, significant cooling drift rates (at times) were observed even though theoretical calculations showed that a significant heating drift rate of 150 μK/min (0.18 Gy/min) would be present at the end of 40 min of agitation.

Some causes of the behavior of subsequent drifts result from imperfect "adiabatic" operation. Changes in drifts can also be caused by changes in temperature gradients that result from variations in axial and radial dose rates, effects which will increase as successive runs are made. Therefore, rapid reduction and control of drifts is a vital and time-saving operation.

The effect of non-adiabatic operation is illustrated by the recording shown in figure 6. The small initial drift indicated near equilibrium conditions, switch S_1 open (fig. 4). A broad cobalt-60 beam was turned on for 90 s, switch S_0 open (fig. 1). Figure 6 indicates that the polystyrene discs rose higher in temperature, ΔT_p, compared to the surrounding water that rose less in temperature, ΔT_w. This caused rapid and non-linear cooling after irradiation, as shown by the recording.

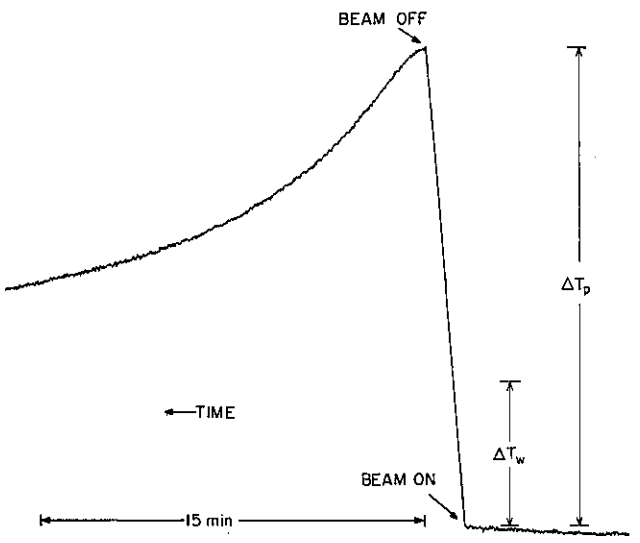

Figure 6–Recording of a non-adiabatic run of 90 s irradiation. The temperature rises of the polystyrene discs and surrounding water are indicated by ΔT_p and ΔT_w, respectively.

Figure 7 illustrates the basic idea of rapidly decreasing and balancing drifts by use of the RC circuit shown in figure 4. Consider switches S_1 and S_2 initially open. The 10-turn, 10-kΩ potentiometer, R_2, was adjusted to about mid-scale and then S_2 was momentarily closed across the 4-μF polystyrene capacitor. The circuit was then connected to the bridge by closing S_1. Assuming that there are no temperature drifts, the bridge output signal will indicate a zero signal as illustrated by the baseline segment OA in figure 7. If R_2 is adjusted to give signal AB or AC, the signal will decay to the baseline at a

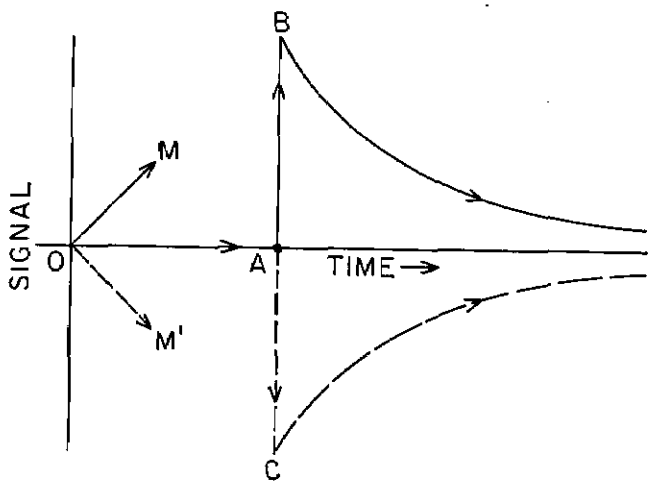

Figure 7–Illustration of the principle used in balancing drifts in electrical signals caused by temperature gradients within the calorimeter.

rate depending mainly on the value of R_3C_1. In this way, a changing external electrical signal was applied across input PP′ of the amplifier input (or output) to oppose a drift in electrical signal caused mainly by internal temperature gradients. For example, an increasing signal produced by a heating temperature drift in the general direction of OM (fig. 7) will be opposed by a decrease of the electrical signal AB. And a decreasing signal produced by a cooling temperature drift in the direction of OM′ will be opposed by a decay of the electrical signal AC.

The RC circuit was adjustable to balance a large range of electrical signal drifts. The resistor R_3 was adjustable to give four resistance values from 0.1 to 1.0 GΩ. This gave time constants of 7, 13, 33, and 67 minutes. The potential V was adjustable in order to place from one to four 1.35-volt mercury cells in series. The maximum electrical drift that could be produced at the amplifier input was equivalent to an absorbed dose rate drift near 7.6 Gy/min in the (C+J) mode, when 4.5 μW of electrical power was dissipated in each thermistor. However, during measurements only small adjustments were needed as will be illustrated below.

Although the RC circuit can greatly reduce observed drifts, it is always good practice to reduce internal temperature gradients as much as possible so that only a small and remaining drift needs to be balanced. This allows more linear drifts which lessen extrapolation errors when analyzing runs. This condition will also permit longer and more accurate irradiation runs, particularly when measuring low dose rates. A large drift observed over a small time at a reduced amplifier gain may appear to be linear; and although the RC circuit will oppose the large drift, the remaining drift might appear to have an objectionably large curvature, particularly when observed under measurement conditions that require a high amplifier gain. Therefore, a way to improve this situation is mainly to decrease the internal temperature gradients.

Reduction of internal temperature gradients in the stagnant water was accomplished in a simple manner. Switch S_1 was open. A heating drift generally meant that heat was conducted from the warmer surrounding water to the cooler polystyrene discs. This drift was reduced by momentary irradiation which raised the temperature of the discs at a rate nearly 3.3 times greater than the surrounding water (switch S_0 of fig. 1 remaining open). This procedure was repeated in steps until the drift was desirably small. Conversely, a cooling drift was reduced by momentarily closing switch S_0 (no beam irradiation), and the procedure was repeated until the drift was also desirably small. After each of these procedures, reasonably short periods of waiting were required to allow for approximate temperature equilibration between the discs and surrounding water. When the drifts are reduced to reasonably small values, further application of these procedures may result in an uneconomical use of time. At this point the RC-circuit can be put into use. Some delayed control of small drifts can be made during measurements by making required adjustments in the adiabatic power controller (fig. 1).

10. Performance

Figure 8 shows the performance of the calorimeter. Time increases from right to left. The initial upward drift shown was considered too large. This heating drift signal was reduced by merely adjusting R_2 to cause the recorder pen to move *in the direction* of the

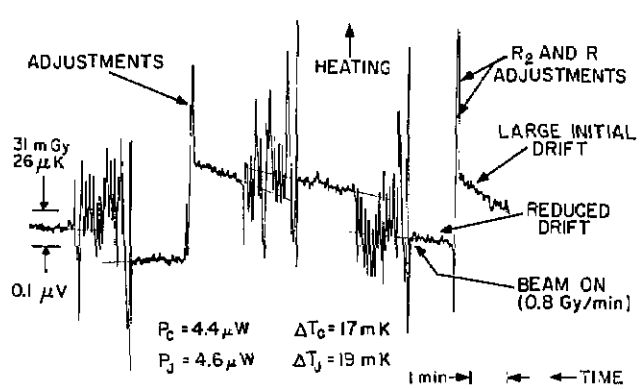

Figure 8–Recorder tracings illustrating quickly balanced electrical signal drifts, large signal-to-noise ratio, and the rapidity of measurements.

drift (upward).[5] Then an adjustment was made by changing the Wheatstone bridge balancing resistor, R, causing the pen to move approximately to the chart mid-scale (the null position). The result shows a much reduced drift signal; and although it could easily have been reduced further, it was considered negligible compared to the beam response. Then switch S_0 (fig. 1) was closed and the beam was immediately turned on. R was adjusted around the null (mid-scale) until S_0 was opened and the beam turned off after 90 s. The abrupt spikes shown are the result of this manual change in R. Two runs were made before further adjustments were made in R_2 and R.

The beam dose rate was near 0.8 Gy/min which produced a 1.0 mK temperature rise in 90 s. This is small compared to the average 18 mK temperature rise of the thermistors as a result of an average electrical power dissipation of 4.5 μW.[6] The total pen deflection during a run was 41 times greater than the indicated distance for 31 mGy. The electrical noise was small.

Figure 8 illustrates control of only small temperature drift signals, up to 17 μK/min. Tests (not shown) indicated that much larger temperature drifts were also reduced and balanced by the RC circuit. The simplicity of the circuit and its ease of use are desirable features for applying it to other calorimeters, in general. (A complicated circuit could be designed to reduce drifts during runs by generating feedback ramp signals predicted by curve fits to background drifts.)

Experience with the calorimeter has shown its utility. Positioning the empty calorimeter, filling it with water to an accurate depth, getting it into operation, and making 30 runs of 100 s duration for each irradiation required about 4 hours.

Insignificant temperature effects were caused in the thermistors as a result of adjusting R_2 in the drift balancer. In figure 8, the first shown adjustment in R_2 produced an initial potential change across PP′ (in fig. 4) of about 0.4 μV. This caused a power change of 15×10^{-6} μW in each thermistor. The temperature change was $(4.1)(15\times10^{-6})$ mK$=0.06$ μK. This is small compared to the noise level which can be estimated as an equivalent temperature change of several microkelvin by use of the illustrated temperature scale shown at the left in figure 8. Furthermore, about 95 percent of the additional 0.06 μK temperature change, caused by that sudden change in R_2, occurred in about 5 s—thereafter a slowly changing drift (theoretically) remained (the behavior would closely resemble that shown in fig. 14 in [5]). Therefore (as a result of adjusting the drift balancer) the effects of the temperature perturbations in the thermistors were essentially non-existent, $<0.001\%$ of the temperature rise caused by irradiation.

11. Results

Figure 9 shows a plot of the measured absorbed dose rates in polystyrene as a function of accumulated absorbed dose. The measurements were made over a 42-day period (the water was drained from the calorimeter after each day of measurement). The measurements were corrected for cobalt-60 decay to the first day of measurement. Each data point

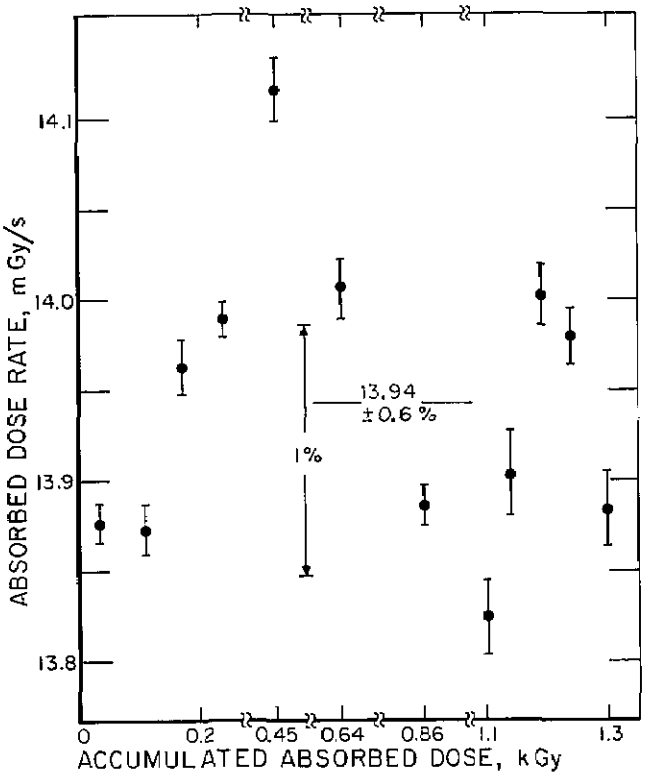

Figure 9–Plot of average results (with mean errors) of daily measurements of polystyrene absorbed dose rate as a function of accumulated absorbed dose. The standard deviation of the shown points is 0.6%,

[5] *The effect of superimposing the exponentially decaying signals* ($R_3C_1=13$ minutes) on the linear drifts resulted in a theoretical error of $<0.01\%$—for the runs shown in figure 8.

[6] Within 3%, each thermistor rose in temperature by 4.1P mK, where P is the thermistor power dissipation in μW. Tests showed that when either thermistor changed in temperature by δT, as a result of a change in P, it produced a temperature change of 0.044 δT in the other thermistor—as determined by the rebalance of the Wheatstone bridge.

represents an average result of 30 to 63 runs (each 90 to 120 s of irradiation), which resulted in an accumulated absorbed dose of 40 to 79 Gy for each group of runs. Each data point is shown plotted against the total absorbed dose the detector received—the sum it received on previous days plus the average it received on the day of measurement. The breaks shown in the abscissa indicate from 150 to 200 Gy of continuously delivered but unmeasured absorbed dose. The total absorbed dose was 1.33 kGy.

The individual runs (not shown) were plotted in all the groups. They showed increases or decreases, of questionable significance, with accumulated dose. The extremes of the changes varied from about a 1.5% increase on the first day to about a 2% decrease on another day. The detector received no irradiation prior to the first day of measurement. The 1.5% increase on the first day occurred up to an accumulated dose of about (30–40) Gy where a plateau was reached. The plateau extended to an accumulated dose of 70 Gy, at the end of the first day of measurement.

There was no consistent evidence of significant effects on measurements of absorbed dose when, on 3 days, measurements were made with six different dissipations of thermistor electrical power (P_C and P_J) that ranged from 4.5 to 320 μW.[7] Measurements in the C-mode (P_C=9 μW while P_J was 0, 9, or 160 μW) gave the same result as measurements in the J-mode (P_J=9 μW while P_C was 0, 9, or 160 μW).

Because there appeared to be no effect due to the various measurement conditions described, and even though the data on some days showed small variations, all the shown plotted data indicate an average of all measurements on a particular day. The uncertainties shown in figure 9 are standard errors of the mean that varied from 0.08 to 0.18%. The computed standard deviation of each group of runs ranged from 0.5 to 1.0% with an average of 0.7%. The plotted results shown in figure 9 were assumed to be random fluctuations about a constant value (no evidence of a continuous and significant change in heat defect). An equal weight was assigned for the average result of each group. Averaging the 12 groups gives 13.94 mGy/s with a standard error of the mean of 0.17%. The 12 average daily values (shown by the points) give a standard deviation of 0.6%. Different averages of nine daily groups of measurements made with the water calorimeter give a standard deviation of 0.2% (fig. 20 in [5]) for the average daily reproducibility.

[7] This contrasts with a nearly 4% change in the measured absorbed dose in the water calorimeter when powers were changed from 9 to 200 μW (fig. 13 in [5]). Also, even at the 320 μW presently used, no change in response was noted as a result of small changes in room air pressure—previously observed. Perhaps the speculative reasons given there (in section 18 in [5]) were correct, concerning the existing conditions and suggested changes (applied to the present detector) of the thermistor and lead embedments described in section 4 of the present paper. Further investigations will be made.

12. Absorbed Dose to Water

The absorbed dose rate in polystyrene, $\dot{D}_p$, produced by gamma rays from a cobalt-60 source, is converted to absorbed dose rate in water, $\dot{D}_w$, by evaluating the equation [22]:

$$\dot{D}_w = \frac{(\bar{\mu}_{en}/\rho)_w}{(\bar{\mu}_{en}/\rho)_p} \cdot P_{repl} \cdot \dot{D}_p \quad . \tag{7}$$

The first term is the ratio of the weighted mean, mass energy-absorption coefficients in water to that of polystyrene (weighted with the photon energy fluence) and the second term (P_{repl}) is the replacement factor, to be discussed later.

Table 2 shows values used in determining the first term. Column 1 shows the energy intervals and column 2 shows values of the photon fluence per primary photon at a depth of 5 g/cm^2 [23]. The scattered fluence is shown to be 45% of the primary fluence. Column 3 shows values of the energy per primary photon, which has a mean energy of 1.252 MeV. The total scattered energy is shown to be 0.22 MeV, which is 15% of the total radiation energy at the point of measurement. Columns 4 and 5 show values of the mass energy-absorption coefficients for water and polystyrene, respectively. Their ratios are shown in column 6. Column 7 shows ratios of the mass attenuation coefficients of water to polystyrene. Values of all the coefficients were obtained from [24]. The last column shows values (in percent) of the scattered photon energy contributions to the total absorbed dose in polystyrene. The scattered energy contributes 16% to the measured absorbed dose.

The first term in eq (7) is

$$\frac{(\bar{\mu}_{en}/\rho)_w}{(\bar{\mu}_{en}/\rho)_p} = \frac{Z_w}{Z_p} = 1.033, \tag{8}$$

where $Z = \bar{E}_{pri}(\mu_{en}/\rho)_{pri} + \Sigma \bar{E}_{scatt}(\mu_{en}/\rho)_{scatt}$. Respectively, $\bar{E}_{pri}$ and $\bar{E}_{scatt}$ are the mean energies of the primary photon and of the scattered photons for the intervals shown in column 1. The contribution of the scattered radiation to absorbed dose shown in column 8 is

Table 2. Scattered radiation contributions to absorbed dose at 5 g/cm^2 depth

Photon energy (MeV)	Fluence per primary photon (×100)	Energy per primary photon (×100) (Mev)	$(\mu_{en}/\rho)_w$ (×100) (cm^2/g)	$(\mu_{en}/\rho)_p$ (×100) (cm^2/g)	$\frac{(\mu_{en}/\rho)_w}{(\mu_{en}/\rho)_p}$	$\frac{(\mu/\rho)_w}{(\mu/\rho)_p}$	Contribution to total absorbed dose in polystyrene (%)
	Scatter	Scatter					
0.00–0.10	5.8	0.29	4.155	2.387	1.741	1.141	0.2
0.10–0.20	8.2	1.23	2.762	2.631	1.050	1.039	0.8
0.20–0.30	7.4	1.85	3.079	2.972	1.036	1.036	1.3
0.30–0.40	1.6	0.56	3.236	3.131	1.034	1.034	0.4
0.40–0.50	2.2	0.99	3.289	3.185	1.033	1.033	0.7
0.50–0.60	2.0	1.10	3.292	3.188	1.032	1.033	0.8
0.60–0.70	2.6	1.69	3.264	3.162	1.032	1.033	1.3
0.70–0.80	2.4	1.80	3.225	3.125	1.032	1.033	1.3
0.80–0.90	2.5	2.13	3.179	3.081	1.032	1.033	1.5
0.90–1.00	2.8	2.66	3.126	3.030	1.032	1.033	1.9
1.00–1.10	2.6	2.73	3.072	2.978	1.032	1.033	1.9
1.10–1.20	3.0	3.45	3.017	2.925	1.032	1.033	2.4
1.20–1.25	1.4	1.72	2.976	2.885	1.032	1.033	1.2
	45	22					16
	Primary	Primary					
1.252[a]	100	125.2	2.961	2.871	1.031	1.033	84
	Total	Total					
0–1.252	145	147					100

[a] This is the average primary photon energy.

$$\bar{E}_{scatt}(\mu_{en}/\rho)_{scatt}/Z,$$

where this is evaluated for polystyrene.

The replacement factor, P_{repl}, was calculated as the ratio of the photon energy fluence in an all-water compared to a polystyrene-water calorimeter (at the position of measurement). The difference in photon energy fluence is caused mainly by the front disc, 10 mm thick. A simplified calculation gives

$$P_{repl}=e^{(\mu_p-\mu_w)t}, \tag{9}$$

where μ_w and μ_p are the linear attenuation coefficients (of the average primary photon energy) in water and polystyrene, and t is the thickness of the polystyrene disc. This fraction calculates to be

$$P_{repl}=1.001.$$

A detailed calculation, that includes the scattered spectrum, causes a difference of $<0.01\%$. These calculated results give

$$D_w=1.034\ D_p. \tag{10}$$

This result is insensitive to the shape of the spectrum. The ratio of the μ/ρ values (column 7) is nearly independent of photon energy above approximately 0.1 MeV. The ratio values near unity would result in approximately the same spectrum in the two materials, including in a graphite medium to which the values listed in columns 1 and 2 actually apply ([23], columns 1 and 6 in table 1). The spectrum would vary slowly as a function of depth.

Below 0.1 MeV the listed values in the first row show that although the ratios of coefficients increase sharply, the energy fluence is decreasing at a faster rate. These resulted in the indicated small contribution of 0.2% of the total (primary plus secondary) absorbed dose.

13. Comparison of Calorimeter Results

A comparison of absorbed dose rates to water, determined with three types of calorimeters, is given in table 3. The corrected and final results with the polystyrene-water, graphite, and water calorimeters are shown in the first row. The second row shows standard errors of the mean, in percent. The third row shows comparisons relative to the result determined with the calorimeter constructed of graphite which is known (as for polystyrene) to have an essentially zero heat defect. The result with the graphite calorimeter is

Table 3. Calorimetric determination of absorbed dose to water

	Calorimeter Type		
	Polystyrene-water	Graphite [6,7]	Water [5]
Water dose rate (mGy/s)	17.85	17.76	18.38
Standard error of the mean (%)	0.2	0.05	0.1
Relative dose rate	1.005	1	1.035
Combined uncertainty (%)	1.1	0.6	0.4

in agreement with the result determined with the polystyrene-water calorimeter, within the combined uncertainties shown in the last row. The above results are, however, in disagreement with the results determined with the water calorimeter. These results indicate an exothermic effect of 3–4% in irradiated water.

Measurements in copies of the NBS water calorimeter irradiated with cobalt-60 gamma rays are about 4% higher when compared with those determined with ionization chambers [8,9].

14. Corrections and Uncertainties

Corrections and uncertainties in measurements of source-detector distance and detector depth near 5 g/cm^2 were negligible because of the optical sighting and micrometer measurements that were used. To compare with the water calorimeter results (that was slightly corrected to apply to an exact 5 g/cm^2 detector depth), the present result was decreased by 0.11% to correct to an equivalent electrons-per-unit-area detector depth. Effects of uncertainties in the calibrated temperature probe (1 mK temperature resolution), needed to measure the sensitivities of the thermistors, were negligible. A negligible uncertainty was also assigned to the measurement of the sensitivities of the thermistors, because of the repeatability of the results shown in table 1. To compare the present result with those determined with the water and graphite calorimeters, a correction was made for cobalt-60 decay by using a half-life value of 5.272±0.002 years [25]. The correction factor was near 1.24, with negligible uncertainty. Čerenkov radiation contains wavelengths which are not locally absorbed but are readily transmitted in transparent materials like polystyrene and water. The maximum effect occurs for electrons from about 1–2 MeV. However, even in this range the effect is less than 0.1% of the electron energy loss by combined other effects. Therefore, the effect of Čerenkov radiation can be neglected, regardless of the incident radiation.

Table 4. Uncertainties in absorbed dose rate to water

Source	Estimated uncertainty (%)	
	Random (degrees of freedom) $s_i(\nu_i)$	Other μ_j
Reproducibility of measurement groups (fig. 9)	0.2 (11)	
Heat defect		0.7
Dose-rate conversion, polystyrene to water		
Absorption coefficient ratio [24]		0.3
Low-energy photons		0.5
Specific heat capacity of polystyrene		0.5
Effect of lead resistances		0.05
Beam attenuation of calorimeter lid	0.05 (5)	
Beam exposure timing		0.05

Combined uncertainty $=\sqrt{\Sigma s_i^2+\Sigma\mu_j^2}=1.1\%$.

Table 4 lists uncertainties from sources shown in column 1. The second column lists uncertainties s_i in terms of standard deviations of random measurements, and the numbers in parentheses are the corresponding numbers of degrees of freedom. The first listed source of uncertainty is 0.2%, which is the standard error of the mean for the reproducibility of measurements on different days (from fig. 9). Ionization measurements in a water phantom showed that the aluminum foil and expanded polystyrene of the calorimeter lid decreased the measurements by 0.34%. This correction was made and a 0.05% uncertainty was assigned.

Column 3 lists uncertainties μ_j which are believed to be reasonable estimates of other uncertainties, to be treated as if they are standard deviations. Because of the essentially zero heat defect reported for different particles ([3], p. 14), [12, 13] and because there is only borderline evidence of a small endothermic heat defect (0.67%±0.97% [14]), no correction was applied but a 0.7% uncertainty was assigned. A 0.3% uncertainty was assigned in the energy-absorption coefficient ratios [24]. Although it was shown that the conversion factor (1.034) for converting absorbed dose in polystyrene to water is insensitive to the radiation spectrum, a 0.5% uncertainty was assigned in the event that the spectrum (particularly of low-energy photons) was greatly different from that used in the calculations. A 0.5% uncertainty is assigned for the specific heat capacity of polystyrene. The Pt-Ir leads fused to each thermistor bead had an average calculated resistance of 12 ohms, and the additional copper leads raised the resistance to an average of 27 ohms external to the nominal 3 kΩ resistance within the beads. The wires and thermistors have,

respectively, a positive and negative temperature coefficient of resistance. A calculation showed that the results of measurements had to be increased by 0.98% because of the 27 ohm external resistance—and increased further by 0.07% because that resistance increased slightly during irradiation. A 0.05% uncertainty was assigned. A 0.05% uncertainty was assigned to the beam exposure timing.

The *combined uncertainty* was calculated by using a recently recommended procedure [26]. That uncertainty was obtained by combining in quadrature the uncertainties shown in table 3. The result is 1.1%. Treating the combined uncertainty as if it were a mean error and multiplying it by 2 gives an *overall uncertainty* of 2.2%.

15. Further Investigations

Some other thermal effects were investigated in the calorimeter both as described and in modified form. When the calorimeter was irradiated with cobalt-60 gamma rays, the 10-mm thick discs were sufficient to stop the most energetic electrons emanating from the water. The electron spectrum at the sensors, therefore, was that emanating from polystyrene. From the surface to a depth of about 5 mm the electron spectrum is only slightly changed because of the difference in properties of the two materials. The effect is negligible, based on an approximate thermal diffusion calculation.

Similar effects at higher beam energies can be kept negligible by an easily made modification of securing additional discs to the detector assembly. This is shown in figure 10. Modification (a) shows the detector sandwiched by any necessary array of polystyrene discs separated by narrow gaps. This arrangement reduces the contributions of scattered radiation from the water. It also permits water to be made to flow between the gaps during agitation. Placement or removal of the discs would have little or no effect on the thermistor response shown in figure 5; but the solid-bodied calorimeter (b), with the same external dimensions and detector depth, would require a considerably longer time for the temperature gradients to subside [15]. Also, drift-producing temperature profiles (particularly those caused by successive runs with collimated beams of electrons) can be relatively easily erased in calorimeter (a); but in calorimeter (b) the time required for comparable equilibration would be prohibitively long (an unregulated surrounding temperature would result in delayed and oscillating drifts).

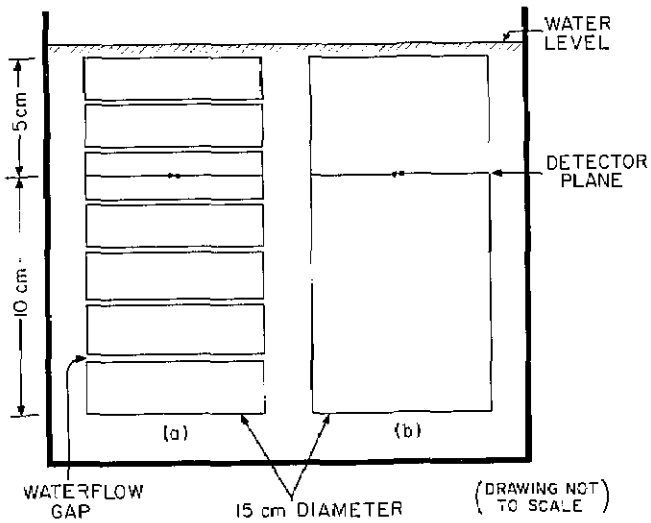

Figure 10–Illustrative modification designs of the polystyrene-water calorimeter.

It is interesting to compare the theoretically calculated changes in drift rates—along the axis at the 5 cm depth, from the top of the uppermost surface to the detector plane (of each calorimeter). It is also convenient to present temperature drift rates as equivalent absorbed dose rates, which is a more meaningful quantity to the operator.

Consider that the entire system (shown in fig. 10) is uniform in temperature. The water is agitated and suddenly raised in temperature by 1 K. Figure 11 shows the changes in drift rates as a function of time.

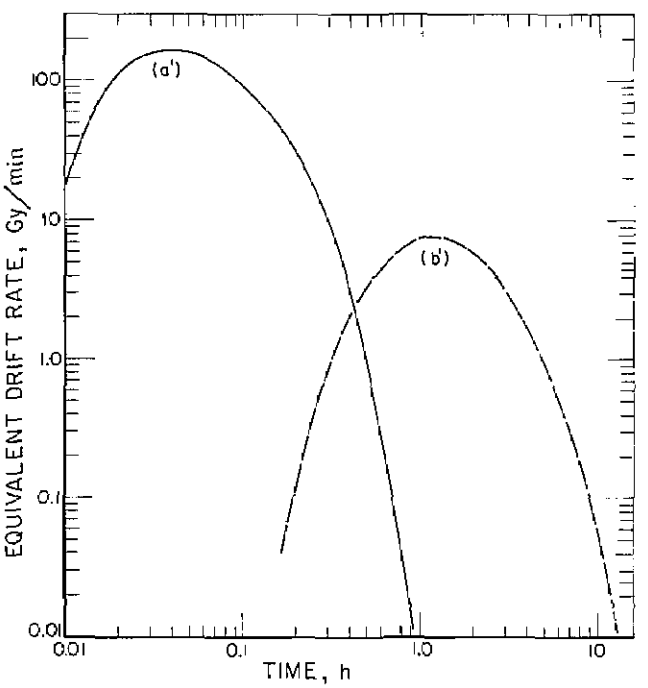

Figure 11–Calculated drift rates caused by thermal diffusion.

Curves (a') and (b') show, respectively, the drift behaviors of calorimeters (a) and (b). Curve (a') indicates that within 1 hour the drift rates would be low enough, <0.01 Gy/min, for calorimeter (a) to operate—verifying what was experienced. In contrast, curve (b') indicates that calorimeter (b) would have large and prolonged drift rates, 1–8 Gy/min from 0.3–5 h.

Section 9 describes the reduction of relatively small but still troublesome internal temperature drifts (in the calorimeter in stagnant water, shown in fig. 1), by use of the immersed electrodes to heat the entire water bath. The use of those electrodes may be ineffective with calorimeter (a). However, effectiveness can be achieved by connecting the electrode leads to other leads that extend into the two gaps adjacent to the detector (along diameters). Varying the electrical power dissipated in those water gaps will change the temperature gradients and will result in a reduction and control of observed temperature drifts. Such a system of heating sections of water (or conductive plastic material) is described in [27].

16. Summary

As with the water [5] and graphite [6] calorimeters, the polystyrene-water calorimeter proved that it can be placed quickly into operation. The mobility of the agitated water quickly brings the calorimeter close to a uniform operating temperature. Remaining temperature drifts were decreased and balanced mainly by use of an RC-circuit placed across a Wheatstone bridge. The charging potential was adjusted in such a manner that the changing electrical signal produced across the bridge was in a direction opposite to that produced by temperature gradients in the calorimeter. Reduction of large internal temperature gradients is important to reducing drifts. Methods for reduction are described.

Positioning the empty calorimeter, filling it with water to an accurate depth, getting it into operation, and making 30 runs of 100 s duration for each irradiation required about 4 hours. A cobalt-60 absorbed dose rate near 14 mGy/s was measured with an uncertainty of about 0.7% standard deviation during a daily set of measurements. Comparison of daily sets of measurements in polystyrene indicated no consistent evidence of a change in heat defect. The accumulated absorbed dose was 1.33 kGy.

The result with the presently described polystyrene-water calorimeter agrees to 0.5% with a result previously determined with a graphite calorimeter (graphite, as for polystyrene, is known to have an essentially zero heat defect). A previous result determined with a water calorimeter is higher by 3–4%, indicating this magnitude of an exothermic effect in water irradiated with cobalt-60 gamma rays.

The study described is part of a second phase of a previously mentioned investigation: the investigation of irradiation effects produced by different beams, absorbed dose rates, and accumulated absorbed dose that may cause significant positive or negative heat defects at a point of measurement—particularly in water which is the standard reference material [3]. The polystyrene-water calorimeter now provides an efficient investigative tool for comparison of the calorimeters under widely different irradiation conditions—conditions where it is uncertain if evidence of an essentially zero heat defect will still exist in polystyrene. To aid in alleviating this concern, and to provide other comparative investigative tools, plans are to design and investigate an A-150 plastic-water and a graphite-water calorimeter. Different models of this general latter design are described in [28] and [29].

In general, the techniques described in this paper can be applied to any material-water calorimeter, to compare the heat defects of those materials for potential calorimetric use, such as a recently developed "solid water" plastic material [30]. Comparison of figure 1 in the present paper with figure 3 in [5] shows that the only differences are the detectors (that are readily interchangeable) and the different roles played by the shown immersed electrodes. The interchangeability provides a convenient feature for comparison of absorbed dose measurements in different materials by making use of a single calorimetric structure and the same measuring equipment. Elimination of a vacuum system, often used with absorbed dose calorimeters, further adds to the simplicity of the basic reported design.

References

[1] Domen, S. R. A polystyrene-water calorimeter. Int. J. Appl. Radiat. Isot. 34(3): 643–644; 1983 March.

[2] Domen, S. R. A temperature-drift balancer for calorimetry. Int. J. Appl. Radiat. Isot. 34(6): 927–928; 1983 June.

[3] ICRU Rep. No. 14, Radiation dosimetry: X rays and gamma rays with maximum photon energies between 0.6 and 50 MeV. Appendix B, ICRU Publications, Washington, DC, 1969.

[4] Domen, S. R. Absorbed dose water calorimeter. Med. Phys. 7(2): 157–159; 1980 March-April.

[5] Domen, S. R. An absorbed dose water calorimeter: Theory, design, and performance, J. Res. Natl. Bur. Stand. (U.S.) 87(3): 211–235; 1982 May–June.

[6] Domen, S. R.; Lamperti, P. J. A heat-loss-compensated calorimeter: Theory, design, and performance. J. Res. Natl. Bur. Stand. (U.S.) 78A(5): 595–610; 1974 September–October.

[7] Pruitt, J. S.; Domen, S. R.; Loevinger, R. The graphite calorimeter as a standard of absorbed dose for cobalt-60 gamma radiation. J. Res. Natl. Bur. Stand. (U.S.) 86(5): 495–502; 1981 September–October.

[8] Marles, A. Comparison of measurements of absorbed dose to water using a water calorimeter and ionization chambers for clinical radiotherapy photon and electron beams. Ph.D. Thesis (1981), Univ. of Texas (Houston).

[9] Kubo, H. Absorbed dose determination with a water calorimeter in comparison with an ionisation chamber. Phys. Med. Biol. (in press).

[10] Boyd, A. W. Private communication, 1981.

[11] Fletcher, J. W. Radiation chemistry of water at low dose rates with emphasis on the energy balance; a computer study. AECL-7834 (Chalk River Nuclear Laboratories, Ontario, Canada); 1982.

[12] Weimer, G. Energiedosisabhängigkeit des kalorischen defekts in kunststoffen. Atomkernenergie 20(4): 327–328; 1972.

[13] Weimer, G. Kalorimetrische dosimetrie schneller neutronen unter berücksichtigung des kalorischen defekts. Dissertation. Giessen: 1. Physikalisches Institut der Universität; 1973.

[14] Säbel, M.; Schmidt, Th.; Pauly, H. Heat defect of low energy x-rays in some materials of interest in absorbed dose calorimetry. Rad. and Environm. Biophys. 11: 259–264; 1974.

[15] Zeitz, L.; Laughlin, J. S. "Nonisolated-sensor" solid polystyrene absorbed dose measurements. Med. Phys. 9(5): 763–768; 1982 September–October.

[16] Gaur, U.; Wunderlich, B. Heat capacity and other thermodynamic properties of linear macromolecules. V. Polystyrene. J. Phys. Chem. Ref. Data, 11(2): 313–325; 1982.

[17] Smathers, J. B.; et al. Composition of A-150 tissue-equivalent plastic. Med. Phys. 4(1): 74–77; 1977 January–February.

[18] McDonald, J. C.; Goodman, L. J. Measurements of the thermal defect for A-150 plastic. Phys. Med. Biol. 27(2): 229–333; 1982 February.

[19] Olson, F. C. W.; Schultz, O. T. Temperatures in solids during heating or cooling. Ind. Eng. Chem. 34(7): 874–877; 1942 July.

[20] Ingersoll, L. R.; Zobel, O. J.; Ingersoll, A. C. Heat conduction. Madison, WI, The University of Wisconsin Press, 299–300 (1954).

[21] Ho, C. Y.; et al. Thermophysical properties of polystyrene and poly (vinyl chloride). Cezairliyan, A., ed. Proceedings of the seventh symposium on thermophysical properties; 1977 May 10–12; Gaithersburg, MD (ASME); 198–218.

[22] Loevinger, R. A formalism for calculation of absorbed dose to a medium from photon and electron beams. Med. Phys. 8(1): 1–12; 1981 January–February.

[23] Comite consultatif pour les etalons de mesure des rayonnements ionisants, Section I—Rayons x et γ, electrons; 2^e Reunion, 1972 May 3–5, Sevres, France, BIPM.

[24] Hubbell, J. H. Photon mass attenuation and energy-absorption coefficients from 1 keV to 20 MeV. Int. J. Appl. Radiat. Isot. 33: 1269–1290; 1982 November.

[25] Hanson, H. H.; Legrand, J. Cobalt-60 decay. At. Energy Rev. 11: 576–641; 1973.

[26] Kaarls, R. Report of the BIPM Working Group on the statement of uncertainties. 1980.

[27] Domen, S. R. Absorbed dose water calorimeter. U.S. Patent Number 4,312,224; 1982 January.

[28] Hohlfeld, K.; Reich, H. Calibration of dose meters in terms of absorbed dose in water for ^{60}Co γ-radiation. Proceedings of an International Symposium on National and International Standardization of Radiation Dosimetry; 1977 December 5–9; Atlanta, GA, Vol. 2: 81–89.

[29] Sundara Rao, I. S.; Naik, S. B. Graphite calorimeter in water phantom and calibration of ionization chambers in dose to water for ^{60}Co gamma radiation. Med. Phys. 7(3): 196–201; 1980 May–June.

[30] Constantinou, C.; Attix, F. H.; Paliwal, B. R. A solid water phantom material for radiotherapy x-ray and γ-ray beam calibrations. Med. Phys. 9(3): 436–441; 1982 May–June.

JOURNAL OF RESEARCH of the National Bureau of Standards
Vol. 88, No. 6, November-December 1983

Applicability of the Colebrook-White Formula to Represent Frictional Losses in Partially Filled Unsteady Pipeflow

J. A. Swaffield and S. Bridge
Brunel University, Uxbridge, Middlesex, U.K.

Accepted: July 19, 1983

The use of Manning's n as a friction factor is shown to be unsuitable in the case of small bore (less than about one meter diameter) partially filled pipeflow, particularly for relatively smooth materials such as glass and cast-iron. The Colebrook-White equation with the roughness coefficient k is presented in a form suitable for inclusion in a computer program to solve the partially filled unsteady pipeflow equations by means of the method of characteristics. Results are presented which show that the Colebrook-White equation provides substantially improved predictions of the wave velocity along the pipe. It provides slightly improved predictions for the maximum depth of flow along the pipe.

Key words: drains; partially filled pipeflow; pipeflow function; plumbing drainage.

1. Introduction

Steady-state flow tests in partially filled pipes on the Brunel test rig at various gradients have shown that the value of Manning's n varies with slope (fig. 1). Similar tests at fixed gradients confirmed results reported elsewhere [2][1] which are that Manning's n also varies with discharge (fig. 2). This is particularly noticeable in channels of circular cross-section. Steady-state tests carried out on 100 mm diameter cast-iron pipe produced values of Manning's n from 0.008 to 0.01, values not significantly different from those found for 100 mm diameter glass pipe. It was felt that these values were too low and were not representative of the roughness of the cast-iron. Manning's coefficient was originally derived for large open channels of rectangular cross-section with fully rough flow. This led to doubts about the validity of using Manning's

About the Authors: J. A. Swaffield heads the Drainage Research Group in the Department of Building Technology at Brunel University where S. Bridge is completing her doctoral program. Dr. Swaffield directs the NBS grant program at Brunel and from time to time since 1980 has conducted research as a guest worker in the Building Equipment Division of the NBS Center for Building Technology.

[1] Figures in brackets indicate literature references at the end of this paper.

Notation

A	cross-sectional area of flow (m^2)
C	Chézy coefficient ($m^{1/2}/s$)
D	pipe diameter (m)
f	Darcy resistance coefficient
g	acceleration due to gravity (m/s^2)
k	roughness coefficient (m)
n	Manning's n ($m^{-1/3}$ s)
Q	discharge (m^3/s)
R	hydraulic radius (m)
Re	Reynold's number (characteristic length equal to the hydraulic radius)
S	channel slope
V	velocity of flow (m/s)
ν	kinematic viscosity of water (m^2/s)

2. The Colebrook-White Equation

The Colebrook-White equation for pipeflow may be written:

$$\frac{1}{\sqrt{f}} = -2 \log_{10} \left[\frac{k}{14.83\,R} + \frac{2.52}{\mathrm{Re}\sqrt{f}} \right]$$

where

f = Darcy resistance coefficient
k = roughness coefficient (m)
R = hydraulic radius (m)
Re = Reynold's number (characteristic length equal to the hydraulic radius)

The Colebrook-White equation for full bore pipeflow may be developed from the general equation by taking the hydraulic radius R to be equal to $D/4$ where D is the pipe diameter in meters. The Chézy equation may be written,

$$V = C\sqrt{RS}$$

where

V = velocity of flow (m/s)
S = channel slope
C = Chézy coefficient $= \sqrt{\frac{8g}{f}}$
g = acceleration due to gravity (m/s^2)

This equation was developed for large open channels and later used to produce Manning's equation, however the effect of cross-sectional channel shape on the Chézy coefficient has been shown to be limited [3] and it may be used for channels which are moderately smooth [1]. Manning's equation is based on the empirical relationship $C = R^{1/6}/n$. Reynold's number is expressed thus,

$$\mathrm{Re} = \frac{4QR}{A\nu}$$

where

Q = discharge (m^3/s)
A = cross-sectional area of flow (m^2)
ν = kinematic viscosity of water (m^2/s)

It is important to use the correct characteristic length for the Reynold's number; here it is the hydraulic radius of flow. From these equations the following expression is derived:

$$Q = \sqrt{32\,gRS}\,A \log_{10} \left[\frac{k}{14.83\,R} + \frac{2.52\nu}{R\sqrt{128\,gRS}} \right] \quad (1)$$

This equation may be used to calculate both normal depth and also the initial steady-state loss.

3. The Roughness Coefficient

The coefficient k is a length parameter characteristic of the surface roughness and is defined as the sand-grain diameter for a sand-coated surface having the same value of f, the Darcy resistance coefficient, as the pipe under consideration. Commenting on Nikuradse's equation for fully rough flow, Henderson [1] says that although it is not easy to determine accurate values of k, this is not a problem since the logarithmic relationship in the equation means that large errors in the value of k produce only small errors in the value of C.

This observation also applies to eq (1) so that slightly inaccurate values of k do not give rise to serious errors in the value of Q. The Transport and Road Research Laboratory Roadnote No. 35 [4] provides a comprehensive list of k values for a wide variety of materials and channel types including the pipe materials currently being used on the Brunel test rig. Glass is generally agreed to be smooth and to have an effective roughness value of zero, cast-iron varies between about 0.1 and 0.3 mm and a value of 0.2 mm was used for the laboratory test pipe. Table 1 gives values for some of the more commonly used pipe materials.

4. Results

4.1 Wave Velocity

Figures 4 and 5 show the time at which the maximum depth occurs along the pipe during the passage of a wave for two different gradients. The graphs compare results from an earlier report ([5], figs.

Table 1. k values for various pipe materials.

Pipe material	k(mm)
Glass	0.0
PVC	0.002
Coated cast-iron	0.1–0.3
Uncoated cast-iron	0.15–0.6
Glazed clay	0.15–0.6

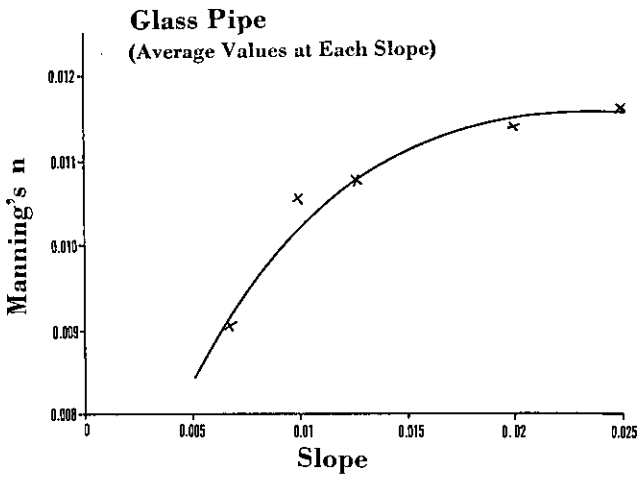

Figure 1–Variation of Manning's n with slope.

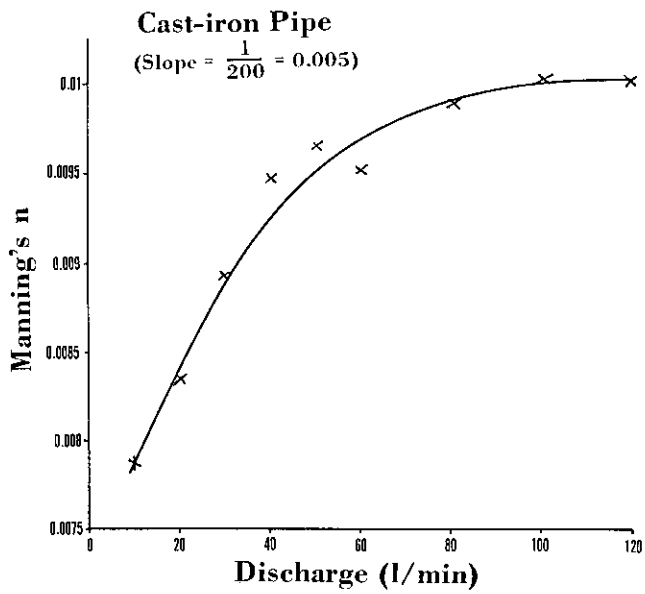

Figure 2–Variation of Manning's n with discharge.

coefficient for small bore partially filled pipeflow, and these doubts were reinforced by the above findings.

The roughness of a pipe is dependent on the flow conditions. If the roughness projections are buried within the laminar sublayer, the pipe is hydraulically smooth; as the laminar sublayer shrinks, the projections assume a greater significance until they break through the sublayer and the flow becomes fully rough. Moderately smooth surfaces such as glass, PVC, cast-iron, etc. produce flows which are in the transitional stage between hydraulically smooth and fully rough flow. Their behavior is described by the Colebrook-White equation [1].

The question of friction factors in open channels was studied by a committee of the American Society of Civil Engineers [3] which found the Colebrook-White equation to be more reliable than the Manning equation with a constant value of n. For any given channel it was found that the roughness value k (used in the Colebrook-White equation) was more likely to be constant than Manning's n. The Colebrook-White equation, unlike Manning's expression, is based on empirical studies of pipeflow and is suitable for partially filled pipeflow provided the surface is moderately smooth hydraulically and the pipe diameter fairly small [1]. Figure 3 shows the change in Manning's n with discharge at two gradients with a fixed value of the roughness coefficient k (the depth for each discharge was found from the Colebrook-White equation and Manning's n calculated using the known depth and discharge) and further demonstrates the variation of the Manning coefficient compared to the roughness coefficient k.

The flow in open channels has long been characterized via experimental data and empirical relationships. Foremost among these relationships is the one associated with the work of Manning giving rise to the roughness coefficient known as Manning's n ([1], pp. 96,101). This technology has since been transferred to the flow of liquids in partially filled conduits.

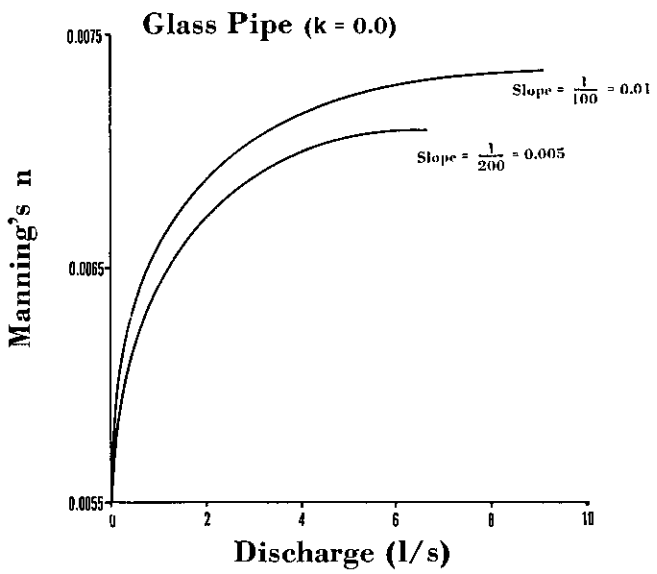

Figure 3–Variation of Manning's n with discharge for a fixed roughness value.

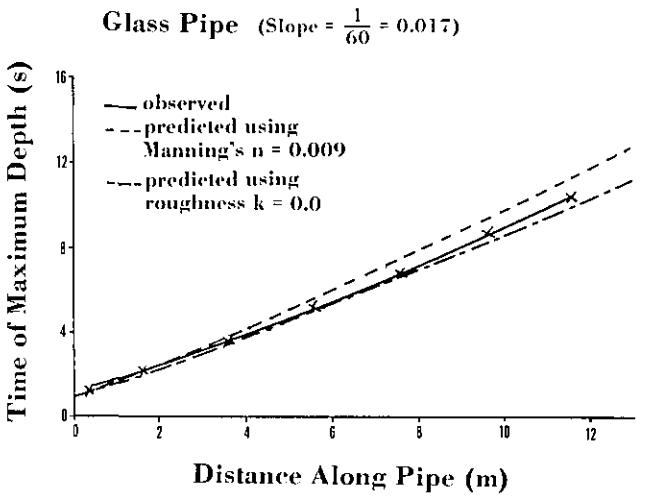

Figure 4–Time of maximum depth versus distance (gradient=1/60=0.017).

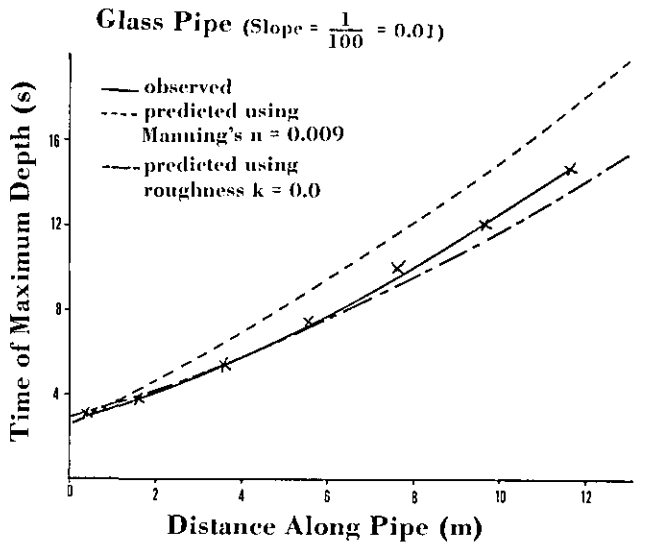

Figure 5–Time of maximum depth versus distance (gradient=1/100=0.01).

6 and 8) using Manning's n with results obtained from running the same data through the program with the Colebrook-White equation for calculating the normal depth and steady-state loss. In both cases the use of the Colebrook-White equation improves the prediction of the velocity of the wave peak along the pipe due to the constancy of the value of the roughness coefficient k with changing depth of flow. Any value of Manning's n used is only valid for one discharge and will therefore over- or under-estimate the loss as the wave travels along the pipe. The Colebrook-White

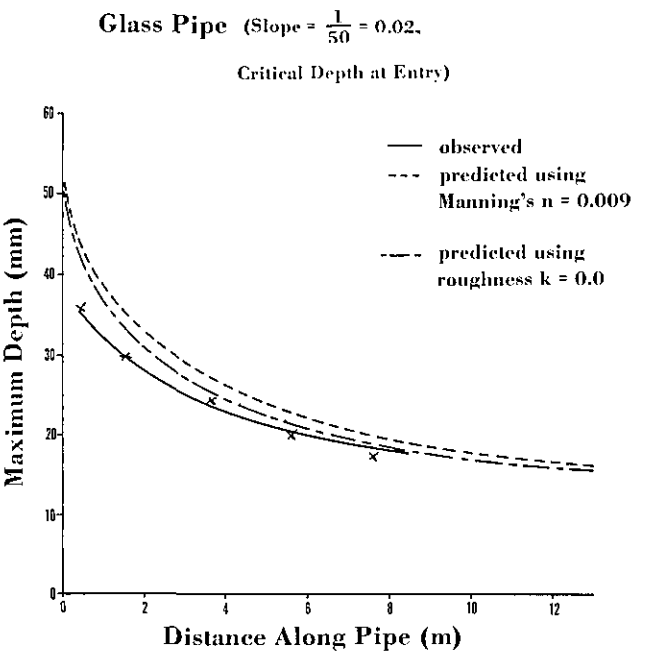

Figure 6–Maximum depth versus distance for glass pipe (gradient=1/50=0.02).

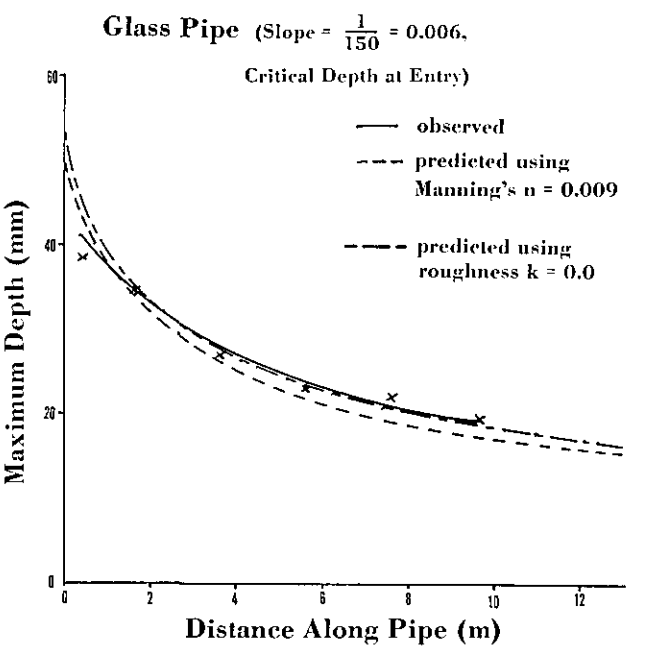

Figure 7–Maximum depth versus distance for glass pipe (gradient=1/150=0.006).

equation allows the loss to be calculated for each node at each time-step, thus significantly reducing the error in estimating the loss.

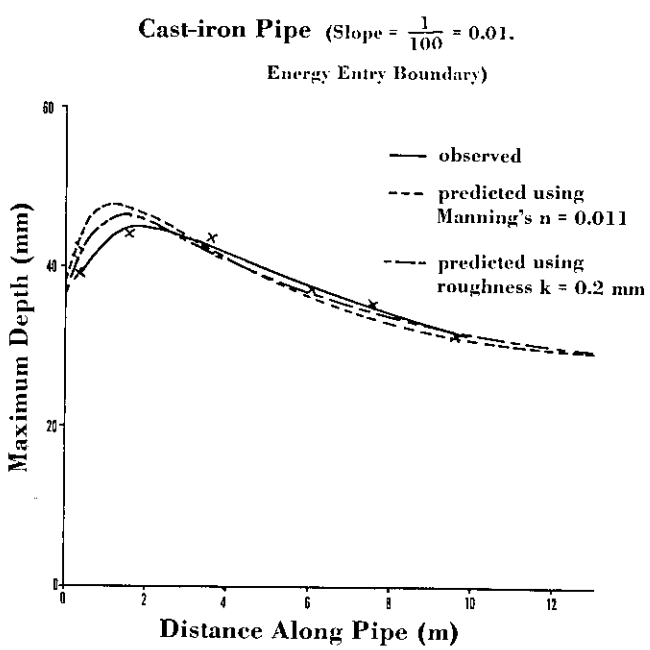

Figure 8–Maximum depth versus distance for cast-iron pipe (gradient=1/100=0.01).

4.2 Maximum Depth

Figures 6 and 7 show the maximum depth of flow as the wave attenuates along the pipe at two different gradients with critical depth at the entry boundary. In both cases the Colebrook-White equation provides a better prediction of the attenuation of the wave, occasionally the improvement is marginal but generally justifies the use of the roughness coefficient k instead of Manning's n. Figure 8 shows the result of a wave from a drop-valve cistern attenuating along a cast-iron pipe, a k value of 0.2 is used and produces a significantly better result than does Manning's equation. The Colebrook-White equation performs far more satisfactorily for the cast-iron pipe than does Manning's equation, which is undoubtedly due to the stability of k over a range of discharge values.

5. Conclusion

The Colebrook-White equation and roughness coefficient k generally predict wave attenuation in both glass and cast-iron pipes with greater accuracy than does Manning's equation. The improvement is particularly noticeable in the prediction of the velocity of the wave peak along the pipe. The variation of Manning's coefficient with both depth and pipe gradient, particularly for circular small-bore pipes (i.e. less than about one meter diameter) highlights the utility of the empirical Colebrook-White equation.

References

[1] Henderson, F. M. *Open Channel Flow.* New York, NY: MacMillan; 1966, 90–101.

[2] Camp, T. R. Design of sewers to facilitate flow. Sew. Works Journal **18**, 1; 1946.

[3] Report, A.S.C.E. task force on friction factors in open channels. Proc. A.S.C.E. **89**, HY2: 97–143; 1963.

[4] Transport & Road Research Laboratory, A guide for engineers to the design of storm sewer systems. T.R.R.L. Roadnote No. 35, H.M.S.O.; 1975.

[5] Swaffield, J. A.; Bridge, S. Experimental vertification of predicted wave attenuation in partially filled drainage pipe-flow. DreG/NBS/1 interim progress report to NBS Washington under grant DA 2004; 1981 June.

JOURNAL OF RESEARCH of the National Bureau of Standards
Vol. 88, No. 6, November-December 1983

Circulants and the Characterization of Vertex-Transitive Graphs*

F. T. Leighton
Massachusetts Institute of Technology, Cambridge, MA 02139

Accepted: September 22, 1982

In this paper, we extend the notion of a circulant to a broader class of vertex-transitive graphs, which we call multidimensional circulants. This new class of graphs is shown to consist precisely of those vertex-transitive graphs with an automorphism group containing a regular abelian subgroup. The result is proved using a theorem of Sabidussi which shows how to recover any vertex-transitive graph from any transitive subgroup of its automorphism group. The approach also allows a short proof of Turner's theorem that every vertex-transitive graph on a prime number of nodes is a circulant.

Key words: circulant; multidimensional circulant; point-symmetric; regular group; starred polygon; vertex-transitive.

1. Introduction

Following the graph-theoretic notation of [10][1] and the group-theoretic notation of [14], we denote the set of nodes of a finite simple graph X by $V(X)$, the set of edges by $E(X)$, and the automorphism group of X by $G(X)$. Throughout, we regard $G(X)$ as a finite permutation group on the nodes, and sometimes the edges, of X. In particular, a subgroup J of $G(X)$ is said to be *transitive* if for every pair of nodes $u,v \in V(X)$, J contains an automorphism mapping u to v. If, in addition to being transitive, $o(J)=o(V(X))$, then J is a *regular* subgroup of $G(X)$. We are interested primarily in those graphs which have a transitive automorphism group. Such graphs are called *vertex-transitive* or, equivalently, *point-symmetric*.

A topic of recent interest in the literature involves the characterization of vertex-transitive graphs [2,3,5,6,8–11,13]. In section 2, we present two such characterizations. The first is elementary and perhaps known to many but we have not found it in the literature. The second is due to Sabidussi [10] and is more substantial. In fact, we present a very slight generalization of his result, which he stated so as to apply only to connected vertex-transitive graphs.

Though Sabidussi's characterization is useful, it involves significant conditions on the automorphism groups of the associated graphs. Indeed, the problem of characterizing vertex-transitive graphs in a more graph-theoretical manner appears to be very difficult. In [13], Turner provided a partial solution to the problem by showing that a graph with a prime number of nodes is vertex-transitive if and only if it is a circulant (or, equivalently, a starred polygon).

About the Author, Papers: F.T. Leighton is an assistant professor of mathematics at MIT and a member of the Laboratory for Computer Science. This paper and the paper following were written while he served as a summer intern at NBS and in part while he was an undergraduate at Princeton University working under the guidance of Professor Stephen B. Maurer.

*AMS(MOS) Subject Classification Numbers: 05C25 20B25 20B10

[1] Figures in brackets indicate literature references at the end of this paper.

Unfortunately, if the number of nodes is not a prime, then a vertex-transitive graph need not be a circulant. In section 3, we define a circulant graph and use the extension of Sabidussi's result to show that a graph X is a circulant if and only if $G(X)$ contains a regular cyclic subgroup. As a corollary, we prove Turner's result mentioned above.

In section 4, we extend the notion of a circulant to a broader class of vertex-transitive graphs, which we call multidimensional circulants. In doing so, we broaden the class of vertex-transitive graphs for which a nice graph-theoretical characterization is known. Moreover, we then give a group-theoretical characterization of what is special about these graphs in relation to the class of all vertex-transitive graphs. In particular, we prove that a graph X is a multidimensional circulant if and only if $G(X)$ contains a regular abelian subgroup. In addition, we derive a simple upper bound on the dimension of a multidimensional circulant and, as an example, prove that the n-cube is an $\lfloor (n+1)/2 \rfloor$-dimensional circulant for $n \geqslant 1$.

2. Characterizations

We now present the characterizations discussed in the introduction. Given any graph X with nodes $V(X)=\{v_0, \ldots, v_{n-1}\}$, define the graph X_i for $0 \leqslant i < n$ to be the subgraph of X induced by $V(X)-\{v_i\}$.

THEOREM 1[2]: *A graph* X *with* n *nodes is vertex-transitive if and only if* $X_0 \simeq X_1 \simeq \ldots \simeq X_{n-1}$.

PROOF: Assume that X is an n-node graph such that $X_0 \simeq X_1 \simeq \ldots \simeq X_{n-1}$. From the definition, we know that $o(E(X_i))=o(E(X))-\deg_X(v_i)$ for $0 \leqslant i < n$, where $o(E(X_i))$ is the number of edges in X_i and $\deg_X(v_i)$ is the degree of node v_i in X. Since $X_0 \simeq X_1 \simeq \ldots \simeq X_{n-1}$, we know that $o(E(X_0))= o(E(X_1))= \ldots =o(E(X_{n-1}))$ and thus that $\deg_X(v_0)=\deg_X(v_1)= \ldots =\deg_X(v_{n-1})$. Thus X is k-regular where $k=\deg_X(v_0)$. This means that each node in X_i has degree k or $k-1$ depending on whether or not the node is adjacent to v_i in X. Let σ_{ij} be an isomorphism from X_i onto X_j. Clearly, σ_{ij} maps the k nodes of degree $k-1$ in X_i (those adjacent to v_i in X) onto the k nodes of degree $k-1$ in X_j (those adjacent to v_j in X). Define the extension of σ_{ij} to X by $\sigma'_{ij}(v_m)=\sigma_{ij}(v_m)$ for $m \neq i$ and $\sigma'_{ij}(v_i)=v_j$. It is clear that for all $0 \leqslant i, j < n$, σ'_{ij} is an automorphism of X mapping v_i onto v_j, and thus X is vertex-transitive.

Conversely, if X is vertex-transitive, then for all i and j, there is a $\sigma \in G(X)$ such that $\sigma(v_i)= v_j$ and thus $\sigma(X_i)=X_j$ which implies that $X_i \simeq X_j$. □

In Theorem 2 of [10], Sabidussi characterizes connected vertex-transitive graphs. We now state a slight generalization of this result to include all vertex-transitive graphs. Given any group G, subgroup J of G and subset H of $G-J$, define $X_{G,H}/J$ to be the graph

$$V(X_{G,H}/J)=\{\alpha J \mid \alpha \in G\} \text{ and}$$

$$E(X_{G,H}/J)=\{(\alpha J, \beta J) \mid \alpha J \cap \beta J \bar{H} \neq \emptyset\}, \text{ where}$$

$$\bar{H}=H \cup H^{-1} \text{ and } H^{-1} \text{ is the set of inverses of elements of } H.$$

THEOREM 2: *If* X *is a vertex-transitive graph and* G *is a transitive subgroup of* G(X), *then there is a subgroup* J *of* G *and a subset* H *of* G–J *such that* $X \simeq X_{G,H}/J$. *Conversely, if* G *is a group,* J *a subgroup of* G *and* H *a subset of* G–J, *then* $X_{G,H}/J$ *is a vertex-transitive graph with* G *homomorphic to a transitive subgroup of its automorphism group.*

The proof of Theorem 2 is lengthy but not difficult and is essentially that found in [10]. We mention here one key step. Given X and G as in the first part of the theorem, choose J to be the subgroup of all automorphisms which fix a given node v_0 and H to be the subset of all automorphisms which move v_0 to an adjacent node.

---

[2] It has been recently discovered that a very similar result was proved by J. A. Bondy in "Reflections on the legitimate deck problem," *Combinatorial Mathematics*, Lecture Notes in Mathematics, No. 686 (1977) 1–13.

3. Circulants

A *circulant* (or equivalently, a *starred polygon*) is a graph whose nodes can be labeled so that there exists a set $S \subset Z$, where Z is the set of integers, such that $V(X)=\{v_0, \ldots, v_{n-1}\}$ and $E(X)=\{(v_i,v_j) \mid 0 \leqslant i,j<n$ and $\text{mod}(i-j,n) \in S\}$. (By $\text{mod}(x,y)$ we mean the remainder of x upon division by y.) For such a graph, the pair (n,S) is called a *symbol* for X. Note that $0 \notin S$ since we are only concerned with simple graphs. Since edges are unordered, we may restrict S so that $d \in S$ if and only if $n-d \in S$ for all values of d. For example, consider the graph in figure 1. Contrary to the claim of Turner [13], this graph is, in fact, a circulant with symbol $(6,\{2,3,4\})$.

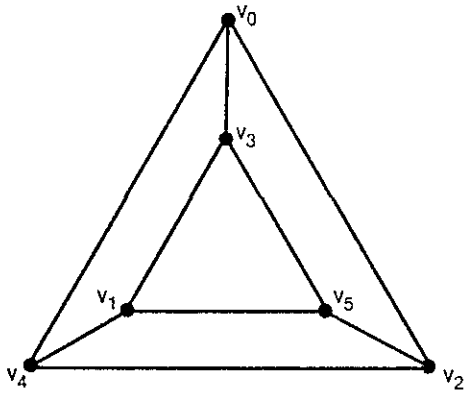

Figure 1

We now determine those vertex-transitive graphs which are circulants. In ([1], Proposition 2), Alspach proves a similar result for tournaments. Henceforth, we assume all subscript arithmetic is done modulo $n=o(V(X))$.

THEOREM 3: *A graph* X *is a circulant if and only if* G(X) *contains a regular cyclic subgroup.*

PROOF: Let X be a circulant with symbol (n,S). Define α to be the permutation $(v_0 v_1 \ldots v_{n-1})$ where $V(X)=\{v_0, \ldots, v_{n-1}\}$. In other words, $\alpha(v_i)=v_{i+1}$ for $0 \leqslant i<n$. Thus $\alpha(E(X))=E(X)$, which means that $\alpha \in G(X)$ and $G(X)$ contains the regular cyclic subgroup $\{1,\alpha, \ldots, \alpha^{n-1}\}$.

Now assume that X is an n-node graph and that $G(X)$ contains a regular cyclic subgroup. Let $G=\{1,\alpha, \ldots, \alpha^{n-1}\}$ be this subgroup. By Theorem 2, we know that there exist disjoint H and J such that $X \simeq X_{G,H}/J$. Since $o(G)=n=o(V(X))=o(V(X_{G,H}/J))=o(G)/o(J)$, we must have $o(J)=1$ and thus $J=\{1\}$. This means that we may relabel $V(X)=\{\alpha^i \mid 0 \leqslant i<n\}$ and $E(X)=\{(\alpha^i,\alpha^j) \mid \alpha^i=\alpha^j\alpha^k$ for some $\alpha^k \subset \bar{H}=H \cup H^{-1}\}$. Note that $\alpha^i=\alpha^j\alpha^k$ if and only if $\text{mod}(i-j,n)=k$. Define $S=\{k \mid \alpha^k \subset \bar{H}\}$. Relabeling the nodes of X once more, we have $V(X)=\{v_0, \ldots, v_{n-1}\}$ and $E(X)=\{(v_i,v_j) \mid \text{mod}(i-j,n) \in S\}$. Thus X is a circulant with symbol (n,S).□

It is now easy to prove Theorem 1 of [13].

THEOREM 4: *A graph with a prime number of nodes is vertex-transitive if and only if it is a circulant.*

PROOF: Let X be vertex-transitive with a prime number p of nodes. Since the subgroup of automorphisms of X which fix a particular node has index p in $G(X)$, $p \mid o(G(X))$. By Sylow's theorem on groups, $G(X)$ contains an element of order p. Without loss of generality, this element must be $\alpha=(v_0 \ldots v_{p-1})$ where $V(X)=\{v_0, \ldots, v_{p-1}\}$, since no permutation on p elements with more than one orbit has order p. Thus $R=\{1,\alpha, \ldots, \alpha^{p-1}\}$ is an order p transitive subgroup of $G(X)$. Equivalently, R is a regular cyclic subgroup of $G(X)$ so by Theorem 3, X is a circulant. Since every circulant is vertex-transitive, the converse follows trivially.□

Not every vertex-transitive graph has an automorphism group containing a regular cyclic subgroup. For example, consider the graph in figure 2. This graph is vertex-transitive but has no automorphism of order eight and thus cannot be a circulant.

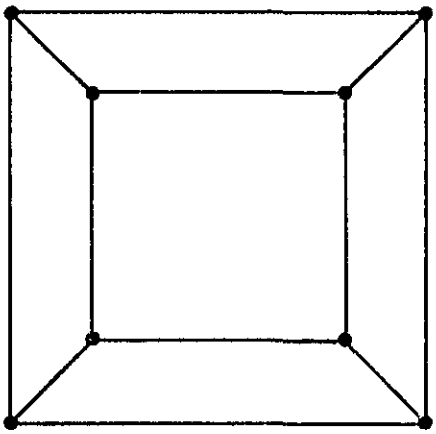

Figure 2

4. Multidimensional Circulants

Define a *multidimensional circulant* to be a graph X whose nodes can be labeled so that there exist positive integers $k, a_1, a_2, \ldots, a_k$ and a set $S \subset Z^k$ such that

$$V(X)=\{v_{i_1, \ldots, i_k} | 0 \leqslant i_l < a_l \text{ for } 1 \leqslant l \leqslant k\} \text{ and}$$

$$E(X)=\{(v_{i_1, \ldots, i_k}, v_{j_1, \ldots, j_k}) | (\text{mod}(i_1-j_1, a_1), \ldots, \text{mod}(i_k-j_k, a_k)) \in S\}.$$

In order to simplify the notation when dealing with multidimensional circulants, we will henceforth employ vector notation. For example, we use the k-vector $\mathbf{a}$ to represent $(a_1, \ldots, a_k)$, $\mathbf{i}$ to represent $(i_1, \ldots, i_k)$, $\mathbf{j}$ to represent $(j_1, \ldots, j_k)$, and so on. In particular, we represent the zero vector $(0, \ldots, 0)$ by $\mathbf{0}$ and the unit vector $(0, \ldots, 0,1,0, \ldots, 0)$ with a one in the ith position and zeros elsewhere by $\mathbf{e}_i$. In addition, it will be convenient to use $\text{mod}(\mathbf{i}-\mathbf{j}, \mathbf{a})$ to represent the k-vector $(\text{mod}(i_1-j_1, a_1), \ldots, \text{mod}(i_k-j_k, a_k))$, $\sigma^{\mathbf{i}}$ to represent the product $\prod_{l=1}^{k} \sigma_l^{i_l}$, and $\mathbf{0} \leqslant \mathbf{i} < \mathbf{j}$ to denote the fact that $0 \leqslant i_l < j_l$ for $i \leqslant l \leqslant k$. Thus a multidimensional circulant is a graph X whose nodes can be labeled so that there exists an integer k, a k-vector $\mathbf{a}$, and a set $S \subset Z^k$ such that

$$V(X)=\{v_{\mathbf{i}} | \mathbf{0} \leqslant \mathbf{i} < \mathbf{a}\} \text{ and}$$

$$E(X)=\{(v_{\mathbf{i}}, v_{\mathbf{j}}) | \text{mod}(\mathbf{i}-\mathbf{j}, \mathbf{a}) \in S\}.$$

Generalizing the concept of a symbol, we define the pair $(\mathbf{a}, S)$ to be a *k-symbol* of X. As was true in the definition of a circulant (where $k=1$), it is clear that the symbol can be restricted so that $\prod_{i=1}^{k} a_i = n = o(V(X))$, $\mathbf{0} \notin S$, $S \subset \{\mathbf{i} | \mathbf{0} \leqslant \mathbf{i} < \mathbf{a}\}$, and that $\mathbf{i} \in S$ if and only if $\text{mod}(-\mathbf{i}, \mathbf{a}) \in S$. For example, consider the graph displayed in figure 2. Whereas this graph is not a circulant, it is a multidimensional circulant. In figure 3a, we display the labeling of this graph which corresponds to the 2-symbol $((2,4),\{(0,1),(0,3),(1,0)\})$, and in figure 3b, we display the labeling which corresponds to the 3-symbol $((2,2,2),\{(0,0,1),(0,1,0),(1,0,0)\})$.

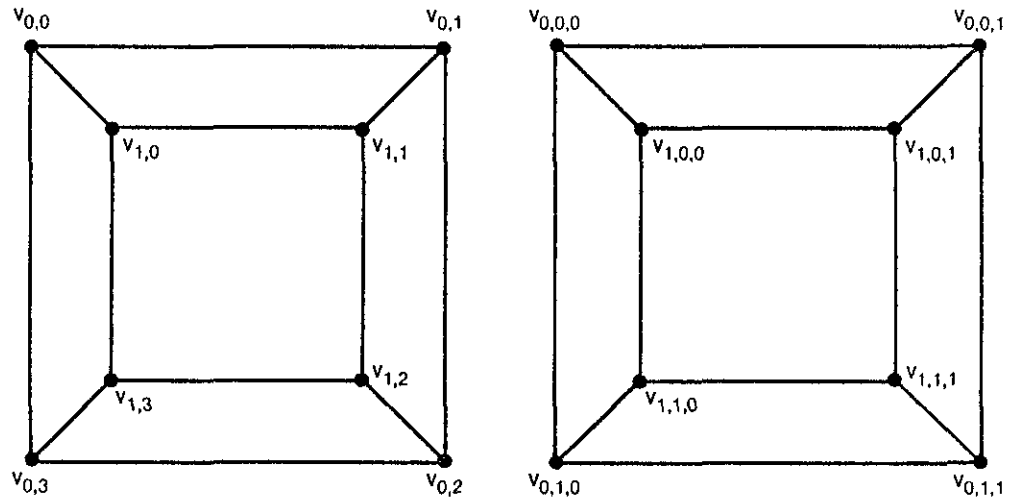

Figure 3

As is evidenced by this example, multidimensional circulants may have k-symbols for several differing values of k. We call the smallest value of k for which a k-symbol exists the *dimension* of the graph. In particular, a graph is said to be a *k-dimensional circulant* if it is a multidimensional circulant and k is the smallest integer for which the graph has a k-symbol. In this notation, the class of circulants is precisely the class of 1-dimensional circulants.

We now generalize Theorem 3.

THEOREM 5: *A graph* X *is a multidimensional circulant if and only if* G(X) *contains a regular abelian subgroup.*

PROOF: Assume that X is a multidimensional circulant with a k-symbol $(\mathbf{a},S)$. Define the permutation σ_l on X for $1\leqslant l\leqslant k$ by $\sigma_l(v_i)=v_{\mathrm{mod}(\mathbf{i}+\mathbf{e}_l,\mathbf{a})}$ for all $v_i\in V(X)$. Since $\mathrm{mod}(\mathrm{mod}(\mathbf{i}+\mathbf{e}_l,\mathbf{a})-\mathrm{mod}(\mathbf{j}+\mathbf{e}_l,\mathbf{a}),\mathbf{a})=\mathrm{mod}(\mathbf{i}-\mathbf{j},\mathbf{a})$, we know that $\sigma_l(E(X))=E(X)$. Thus, $\sigma_l\in G(X)$ for $1\leqslant l\leqslant k$. Further, $\sigma_l\sigma_m=\sigma_m\sigma_l$ for $1\leqslant l,m\leqslant k$ and, thus, the subgroup of $G(X)$ generated by $\{\sigma_1,\ldots,\sigma_k\}$ is abelian. It is not difficult to show that this subgroup is also transitive and has $\prod_{i=1}^{k} a_i=o(V(X))$ elements. Thus it is regular and we have shown that $G(X)$ contains a regular abelian subgroup.

Now assume that we are given a graph X such that $G(X)$ contains a regular abelian subgroup R. By a well-known result concerning finitely generated abelian groups ([4], p. 101–3), we know that we can express R as the direct product of cyclic groups. Thus we can write $R=\bigtimes_{i=1}^{k} R_i$ where each R_i is cyclic, has order a_i, and is generated by σ_i. Replacing G with R in Theorem 2, we know that there exist $H\subset R-\{1\}$ and a subgroup J of R such that $X\simeq X_{R,H}/J$. Since R is regular, we must have that $J=\{1\}$. Thus we may label the nodes of X so that

$$V(X)=\{\sigma^{\mathbf{i}}\mid 0\leqslant\mathbf{i}\leqslant\mathbf{a}\}\text{ and}$$
$$E(X)=\{(\sigma^{\mathbf{j}},\sigma^{\mathbf{i}})\mid\sigma^{\mathbf{i}}=\sigma^{\mathbf{j}}\sigma^{\mathbf{h}}\text{ for some }\sigma^{\mathbf{h}}\in\bar{H}\}.$$

Since R is abelian, $\sigma^{\mathbf{i}}=\sigma^{\mathbf{j}}\sigma^{\mathbf{h}}$ if and only if $\sigma^{\mathbf{i}-\mathbf{j}}=\sigma^{\mathbf{h}}$ and thus if and only if $\mathrm{mod}(\mathbf{i}-\mathbf{j},\mathbf{a})=\mathbf{h}$. Further simplifying, it is possible to relabel the nodes of X so that

$$V(X)=\{v_{\mathbf{i}}\mid 0\leqslant\mathbf{i}<\mathbf{a}\}\text{ and}$$
$$E(X)=\{(v_{\mathbf{i}},v_{\mathbf{j}})\mid\mathrm{mod}(\mathbf{i}-\mathbf{j},\mathbf{a})\in S\}$$

where $S=\{\mathbf{h}\mid\sigma^{\mathbf{h}}\in\bar{H}\}$. Thus X is a multidimensional circulant with k-symbol $(\mathbf{a},S)$.□

COROLLARY 1: Every multidimensional circulant is vertex-transitive.

The arguments in the preceding proof make it clear that, in principle, it is possible to determine the dimension of a multidimensional circulant through examination of the structure of its automorphism group. In practice, however, this may be quite difficult to accomplish. The following theorem provides an upper bound on the dimension based solely on the number of nodes in the graph.

THEOREM 6: *If* X *is a multidimensional circulant with* $n = \prod_{i=1}^{t} p_i^{b_i}$ *nodes (primes* $p_i \neq p_j$ *for* $i \neq j$*), then* X *has dimension* k *for some* $k \leqslant \max_{1 \leqslant i \leqslant t}(b_i)$.

PROOF: Given a multidimensional circulant X, we know from Theorem 5 that $G(X)$ contains a regular abelian subgroup R. Decomposing R into cyclic subgroups, we have $R = \bigtimes_{i=1}^{t} \bigtimes_{j=1}^{d_i} R_{ij}$ where R_{ij} is a cyclic subgroup of R with order $p_i^{c_{ij}}$. Recomposing cyclic subgroups with differing prime power orders, we can write $R = \bigtimes_{j=1}^{\max d_i} R'_j$ where R'_j is cyclic with order $\prod_{i=1}^{t} p_i^{c_{ij}}$ (c_{ij} is defined to be zero if $j > d_i$) and is the product (with as many terms as exist) $R_{1,j} \times \ldots \times R_{t,j}$. Thus R is the direct product of $\max_{1 \leqslant i \leqslant t}(d_i)$ cyclic subgroups. The result now follows from the arguments in the proof of Theorem 5 and the fact that $d_i \leqslant b_i$ for $1 \leqslant i \leqslant t$.□

COROLLARY 2: The class of n-node multidimensional circulants is precisely the class of n-node circulants whenever n is the product of disjoint primes.

We now demonstrate the existence of k-dimensional circulants for every $k \geqslant 1$. This is accomplished by showing that the n-cube is an $\lfloor (n+1)/2 \rfloor$-dimensional circulant for every $n \geqslant 1$. The *n-cube* is the graph X with nodes $V(X) = \{v_i \mid 0 \leqslant i < 2^n\}$ and edges $E(X) = \{(v_i, v_j) \mid$ the n-bit binary representation of i differs from the n-bit binary representation of j in exactly one bit$\}$. The 3-cube, for example, is displayed in figures 2 and 3. Our result requires the following lemma, the proof of which was suggested by Lawrence [7].

LEMMA 1: *If* α *is an element of a regular abelian subgroup of automorphisms of the* n*-cube, then* α *has order* 1, 2, or 4.

PROOF: Let R be any regular abelian subgroup of automorphisms of the n-cube X. View R as an automorphism subgroup of the facets of X. The *facets* of X are the $(n-1)$-cubes contained in X. There are $2n$ such $(n-1)$-cubes, one corresponding to each set of 2^{n-1} nodes whose labels have identical ith bits for some fixed i, $1 \leqslant i \leqslant n$, in the n-bit binary representation of the labels. It is not difficult to show that the action of an automorphism on the facets of X completely determines its action on the nodes, and vice-versa.

Let $F_1, \ldots, F_k$ be the facet orbits of R and define R_i for $1 \leqslant i \leqslant k$ to be the restriction of R to F_i with duplicates eliminated. Then, each R_i is a group of automorphisms of F_i and $R \subseteq \bigtimes_{i=1}^{k} R_i$. Thus $o(R) \leqslant \prod_{i=1}^{k} o(R_i)$ and, since $o(R) = 2^n$,

$$\prod_{i=1}^{k} o(R_i) \geqslant 2^n. \tag{1}$$

In addition, each R_i is regular on F_i. If not, then we could find $s,t \in F_i$ and $\alpha,\beta \in R_i$ such that $\alpha(s) = s$, $\alpha(t) \neq t$ and $\beta(s) = t$. By the commutativity of R, this implies $t = \beta(s) = \alpha\beta\alpha^{-1}(s) = \alpha(t) \neq t$ which is a contradiction. Thus $o(R_i) = o(F_i)$ for $1 \leqslant i \leqslant k$. By definition, we must have $\sum_{i=1}^{k} o(F_i) = 2n$ and thus

$$\sum_{i=1}^{k} o(R_i) = 2n. \tag{2}$$

It is well known that the order of an orbit is a divisor of the order of the permutation group [14]. Thus $o(R_i)|o(R)$ for $1\leqslant i\leqslant k$. Since $o(R)=2^n$, we can define nonnegative integers r_i such that $o(R_i)=2^{r_i}$ for $1\leqslant i\leqslant k$. Rewriting (1) and (2), we have

$$\sum_{i=1}^{k} r_i \geqslant n \quad \text{and} \quad \sum_{i=1}^{k} 2^{r_i}=2n.$$

Thus $\sum_{i=1}^{k} 2r_i \geqslant 2n = \sum_{i=1}^{k} 2^{r_i}$. Since $2r_i<2^{r_i}$ for $r_i=0$ and $r_i>2$ and $2r_i=2^{r_i}$ for $1\leqslant r_i\leqslant 2$, it is clear that $1\leqslant r_i\leqslant 2$ for $1\leqslant i\leqslant k$. Thus $o(R_i)=2$ or 4 for $1\leqslant i\leqslant k$. Thus for each $\alpha\in R$, α^4 leaves each facet of X fixed and $\alpha^4=1$. Thus $o(\alpha)=1$, 2, or 4.□

We are now ready to prove:

THEOREM 7: *The* n*-cube is an* $\lfloor(n+1)/2\rfloor$*-dimensional circulant.*

PROOF: We first show that the n-cube X is a k-dimensional circulant for some $k\leqslant\lfloor(n+1)/2\rfloor$. It follows from the definition of X that we may label the nodes so that X has symbol $(\mathbf{a},S)$ where $\mathbf{a}=(2,2,\ldots,2)$ and $S=\{\mathbf{e}_i\,|\,1\leqslant i\leqslant n\}$. By relabeling node v_i with index $\mathbf{j}$ so that

$$j_l=\left\{\begin{array}{l} 0 \text{ if } (i_{2l-1},i_{2l})=(0,0)\\ 1 \text{ if } (i_{2l-1},i_{2l})=(0,1)\\ 2 \text{ if } (i_{2l-1},i_{2l})=(1,1)\\ 3 \text{ if } (i_{2l-1},i_{2l})=(1,0)\\ i_n \text{ if } 2\nmid n \text{ and } l=\lfloor(n+1)/2\rfloor \end{array}\right\} \qquad \text{for } 1\leqslant l\leqslant\lfloor(n+1)/2\rfloor,$$

it is easy to show that X has $\lfloor(n+1)/2\rfloor$-symbol $(\mathbf{a},S)$ where

$$\mathbf{a}=\left\{\begin{array}{l}(4,4,\ldots,4) \text{ if } 2\,|\,n\\ (4,\ldots,4,2) \text{ if } 2\nmid n\end{array}\right\} \quad \text{and}$$

$$S=\{\pm\mathbf{e}_i\,|\,1\leqslant i\leqslant\lfloor(n+1)/2\rfloor\}.$$

Thus X is a k-dimensional circulant for some $k\leqslant\lfloor(n+1)/2\rfloor$.

Assume now that X has dimension $k<\lfloor(n+1)/2\rfloor$. Then X has a k-symbol $(\mathbf{a},S)$ such that $\prod_{i=1}^{k} a_i=2^n$. But this means that $a_i\geqslant 8$ for at least one value of i. Otherwise, $\prod_{i=1}^{k} a_i \leqslant 4^k\leqslant 4^{(n+1)/2-1}\leqslant 2^{n-1}<2^n$. By the arguments in the proof of Theorem 5, $G(X)$ must contain a regular abelian subgroup with an element of order $a_i\geqslant 8$. But this contradicts the result of Lemma 1. Thus X has dimension $\lfloor(n+1)/2\rfloor$.□

Not every vertex-transitive graph is a multidimensional circulant. Indeed, there are examples of vertex-transitive graphs which do not have a regular subgroup of automorphisms. For instance,

the smallest transitive subgroup of automorphisms of the 10-node Petersen graph, shown in figure 4, has 20 elements.

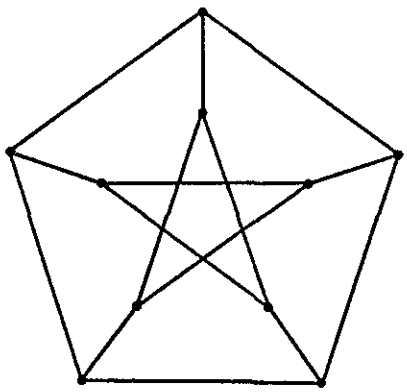

Figure 4

5. Concluding Remarks

With the introduction of multidimensional circulants, we have moderately broadened the class of vertex-transitive graphs for which a nice graph-theoretical characterization is known. The notational complexity, however, has increased substantially. Indeed, the problem of characterizing graph-theoretically the entire class of vertex-transitive graphs has been unsolved for quite some time. Maybe some of the following subclasses are easier to characterize: those with an automorphism group containing a regular subgroup (the Cayley graphs), those with an automorphism group containing an order $o(V(X))$ transitive subset, or those with twice a prime number of nodes. The last subclass has received much attention in the literature of late [3,8,9,11], but even so, a complete characterization has yet to be found.

In addition to Professor Maurer and Dr. Lawrence, the author would like to thank Professors Brian Alspach, Charles Johnson, and Alan Goldman for their helpful remarks.

6. References

[1] Alspach, B. On point-symmetric tournaments. Can. Math. Bull. **13**: 317–323; 1970.
[2] Alspach, B. Point-symmetric graphs and digraphs of prime order and transitive permutation groups of prime degree. J. Comb. Th. (B). **15**: 12–17; 1973.
[3] Alspach, B.; Sutcliffe, R. J. Vertex-transitive graphs of order 2p. 2d Int. Conf. Combinational Math. New York, NY: 18–27; 1978. Ann. NY Acad. Sci. **319**: 1979.
[4] Burnside, W. *The Theory of Groups of Finite Order.* New York: Dover Publications; 1955.
[5] Berggren, J. L. An algebraic characterization of symmetric graphs with p points, p an odd prime. Bull. Aust. Math. Soc. **7**: 131–134; 1972.
[6] Chao, C. On the classification of symmetric graphs with a prime number of vertices. Trans. Am. Math. Soc. **158**: 247–256; 1971.
[7] Lawrence, J. personal communication, unpublished; 1979.
[8] Leighton, F. T. On the decomposition of vertex-transitive graphs into multicycles. J. Res. Natl. Bur. Stand. (U.S.). **88**(6): 403–410; 1983 September–October.
[9] Leighton, F. T. The characterization of vertex-transitive graphs. Senior thesis, Mathematics Department, Princeton University, unpublished; 1978.
[10] Sabidussi, G. Vertex-transitive graphs. Monatsh. Math. **68**: 426–438; 1964.
[11] Sutcliffe, R. J. Vertex-transitive graphs. M.Sc. thesis, Simon Fraser University, unpublished; 1974.
[12] Tuero, M. A contribution to the theory of cyclic graphs. Matrix Tensor Quarterly. **11**: 74–80; 1961.
[13] Turner, J. Point-symmetric graphs with a prime number of points. J. Comb. Th. **3**: 136–145; 1967.
[14] Wielandt, H. *Finite Permutation Groups.* New York: Academic Press; 1964.

JOURNAL OF RESEARCH of the National Bureau of Standards
Vol. 88, No. 6, November-December 1983

On the Decomposition of Vertex-Transitive Graphs into Multicycles*

F. T. Leighton
Massachusetts Institute of Technology, Cambridge, MA 02139

Accepted: September 22, 1982

In this paper, we prove that every vertex-transitive graph can be expressed as the edge-disjoint union of symmetric graphs. We define a multicycle graph and conjecture that every vertex-transitive graph can be expressed as the edge-disjoint union of multicycles. We verify this conjecture for several subclasses of vertex-transitive graphs, including Cayley graphs, multidimensional circulants, and vertex-transitive graphs with a prime or twice a prime number of nodes. We conclude with some open questions of interest.

Key words: Cayley graph; circulant; cycle decomposition; edge-transitive graph; grouplike set; line-symmetric graph; multicycle; multidimensional circulant; point-symmetric graph; starred polygon; symmetric graph; vertex-transitive graph.

1. Introduction

Following the notation of [7,9],[1] we denote the set of nodes of a finite, simple graph X by $V(X)$, the set of edges by $E(X)$, and the automorphism group of X by $G(X)$. Throughout, we regard $G(X)$ as a permutation group on the nodes, and sometimes the edges, of X. In particular, a subgroup J of $G(X)$ is said to be *transitive* if for every pair of nodes $u,v \in V(X)$, J contains an automorphism mapping u to v. If, in addition to being transitive, $o(J)=o(V(X))$, then J is a *regular* subgroup of $G(X)$. It is well known (see Lemma 16.3 of [4], for example) that $G(X)$ contains a regular subgroup if and only if X is a Cayley graph. A *Cayley graph* $X_{G,H}$ is the graph defined by $V(X_{G,H})=\{\alpha \mid \alpha \in G\}$ and $E(X_{G,H})=\{(\alpha,\beta) \mid \alpha\beta^{-1} \in H\}$ where G is an abstract group and H is a subset of $G-\{1\}$ closed under inverses.

We are interested primarily in those graphs with a transitive automorphism group. Such graphs are called *vertex-transitive* or, equivalently, *point-symmetric*. Similarly, a graph is called *edge-transitive* or, equivalently, *line-symmetric* if $G(X)$ is transitive on the *edges* of X. Graphs which are both vertex-transitive and edge-transitive are called *symmetric*. As is pointed out in [4,6,8], not every vertex-transitive graph is edge-transitive nor is every edge-transitive graph vertex-transitive. An area of recent interest in the literature involves the relationship between the class of vertex-transitive graphs and the class of edge-transitive graphs, and the nature of their intersection, the class of symmetric graphs [3–6,8].

About the Author, Papers: F. T. Leighton is an assistant professor of mathematics at MIT and a member of the Laboratory for Computer Science. This paper and the paper preceding were written while he served as a summer intern at NBS and in part while he was an undergraduate at Princeton University working under the guidance of Professor Stephen B. Maurer.

*AMS(MOS)Subject Classification Numbers: 05C25 05A17 20B10 20B25

[1] Figures in brackets indicate literature references at the end of this paper.

Of particular interest is the class of circulants [1,2,7,8,10,11] and a generalization thereof, the class of multidimensional circulants [7,8]. A *circulant* or, equivalently, a *starred polygon* is a graph whose nodes can be labeled so that there exists a set $S \subset Z$, where Z is the set of integers, such that $V(X)=\{v_0, \ldots, v_{n-1}\}$ and $E(X)=\{(v_i,v_j) \mid 0 \leqslant i,j<n$ and $\text{mod}(i-j,n) \in S\}$. (By $\text{mod}(x,y)$, we mean the remainder of x upon division by y.) For such a graph, the pair (n,S) is called a *symbol* for X. In [7], we generalize this concept and define a *multidimensional circulant* to be a graph X whose nodes can be labeled so that there exist an integer k, a k-vector $\mathbf{a}$, and a set $S \subset Z^k$ such that $V(X)=\{v_\mathbf{i} \mid 0 \leqslant \mathbf{i} < \mathbf{a}\}$ and $E(X)=\{(v_\mathbf{i},v_\mathbf{j}) \mid \text{mod}(\mathbf{i}-\mathbf{j},\mathbf{a}) \in S\}$. The pair $(\mathbf{a},S)$ is called a *k-symbol* of X. (We employ the vector notation introduced in [7] whenever discussing multidimensional circulants. In particular, $\mathbf{i}=(i_1, \ldots, i_k)$, $j=(j_1, \ldots, j_k)$, $\mathbf{a}=(a_1, \ldots, a_k)$, $\mathbf{0}=(0, \ldots, 0)$, $\text{mod}(\mathbf{i}-\mathbf{j},\mathbf{a})=(\text{mod}(i_1-j_1, a_1), \ldots, \text{mod}(i_k-j_k, a_k))$, and $\mathbf{0} \leqslant \mathbf{i} < \mathbf{a}$ if and only if $0 \leqslant i_l < a_l$ for $1 \leqslant l \leqslant k$.)

In this paper, we investigate the decomposition of vertex-transitive graphs into edge-disjoint symmetric graphs. In particular, we prove in section 2 that every vertex-transitive graph can be expressed as the edge-disjoint union of symmetric graphs.

In section 3, we define a grouplike set and a multicycle graph and use their properties to extend the result of section 2. We conjecture that every vertex-transitive graph can be expressed as the edge-disjoint union of multicycles. This conjecture is verified for several subclasses of vertex-transitive graphs, including Cayley graphs, multidimensional circulants, and vertex-transitive graphs with a prime or twice a prime number of nodes.

We conclude by mentioning some related problems of interest in section 4. In particular, we show how to construct a multicycle decomposition from the symbol of any multidimensional circulant.

2. Symmetric Graph Decomposition

Let X be any graph, e an edge of X, and G a subgroup of $G(X)$. The *orbit* of e under G is defined as the subgraph $X_{G,e}$ of X which has nodes $V(X)$ and edges $\{\sigma(e) \mid \sigma \in G\}$. The orbits of X possess several well-known and useful properties. We cite three such properties in the following lemmas. The proofs of these lemmas are not difficult and are deferred until section 3, where we prove similar results for a more general subset of $G(X)$.

LEMMA 1: $X_{G,e}$ *is edge-transitive.*

LEMMA 2: $G \subseteq G(X_{G,e})$.

LEMMA 3: X *can be expressed as the edge-disjoint union of the distinct* $X_{G,e}$.

With the use of these lemmas, it is not difficult to prove:

THEOREM 1: *Every vertex-transitive graph* X *can be expressed as the edge-disjoint union of one or more symmetric graphs, each with vertex set* $V(X)$.

PROOF: Let X be any vertex-transitive graph and let $G=G(X)$. Consider the graphs $X_{G,e}$. By definition, they each have vertex set $V(X)$. From Lemma 1, we know that each $X_{G,e}$ is edge-transitive. Since X is vertex-transitive, G must be transitive, and, by Lemma 2, we know that each $X_{G,e}$ is vertex-transitive. Thus, each $X_{G,e}$ is symmetric. Finally, we know from Lemma 3 that X can be expressed as the edge-disjoint union of the distinct $X_{G,e}$.□

3. Multicycle Decomposition

Call a graph a *multicycle* if it can be written as the node-disjoint union of equal length cycles. In particular, for any pair of positive integers b and d, define the multicycle $C_{b,d}$ to be the graph consisting of b node-disjoint d-cycles. Several examples are provided in figure 1. (Note that we have adopted the convention that every edge is a 2-cycle and that every node is a 1-cycle.)

It is not difficult to show that every multicycle is symmetric. We state a partial converse of this fact in the following lemma.

LEMMA 4: *If* X *is a vertex-transitive graph and* $o(E(X)) \leqslant o(V(X))$, *then* X *is a multicycle.*

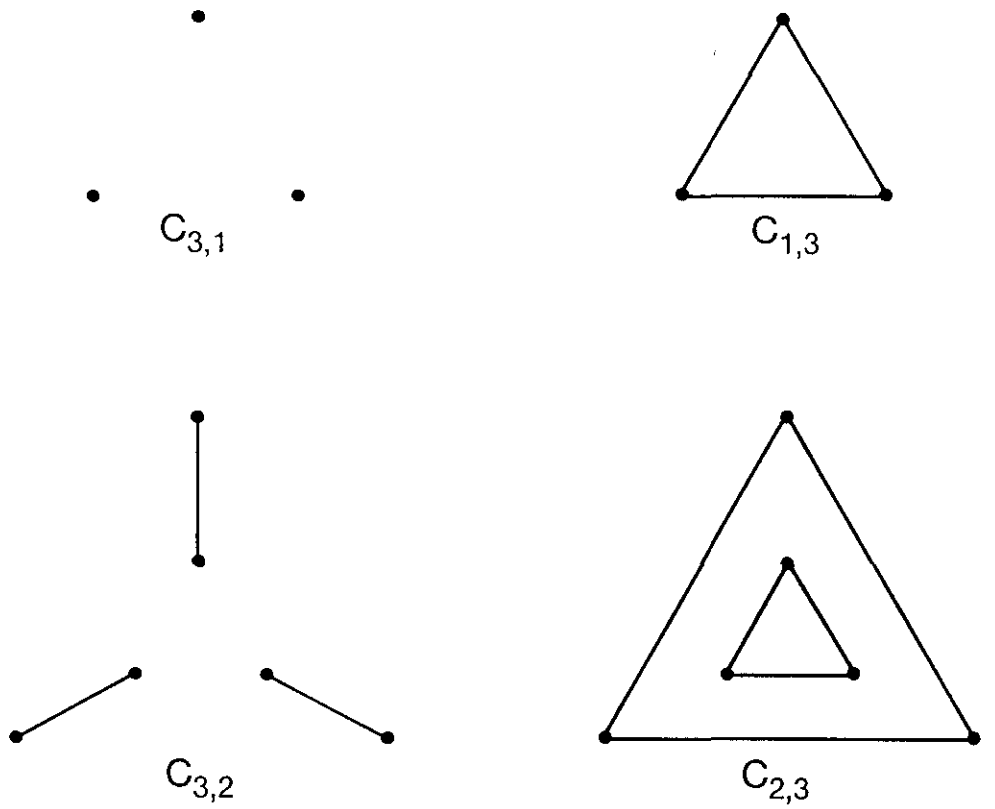

Figure 1

PROOF: Since X is vertex-transitive, all the nodes of X must have the same degree. Since $o(E(X)) \leqslant o(V(X))$, this common degree is 0, 1 or 2. In the first case, $X \simeq C_{n,1}$ where $n = o(V(X))$. In the second case, X consists entirely of node-disjoint edges and $X \simeq C_{n/2,2}$. In the final case, X is the node-disjoint union of cycles and, since X is vertex-transitive, each cycle must have the same length. Thus $X \simeq C_{b,d}$ for some b and d such that $bd = n$.□

We now extend Theorem 1.

THEOREM 2: *Every Cayley graph* X *can be expressed as the edge-disjoint union of multicycles, each with vertex set* V(X).

PROOF: The proof is identical to that of Theorem 1 with an additional observation. Let X be any Cayley graph and let R be a regular subgroup of $G(X)$. By definition, R is transitive and has $o(V(X))$ elements. Thus each $X_{R,e}$ is symmetric and has at most $o(V(X))$ edges. Since $o(E(X_{R,e})) \leqslant o(V(X)) = o(V(X_{R,e}))$ for every $e \in E(X)$, we know by Lemma 4 that each $X_{R,e}$ is a multicycle.□

COROLLARY 1: *Every multidimensional circulant can be expressed as the edge-disjoint union of multicycles. In particular, every vertex-transitive graph with a prime number of nodes can be expressed as the edge-disjoint union of multicycles.*

PROOF: We know from [7] that every vertex-transitive graph with a prime number of nodes is a circulant and that the automorphism group of a multidimensional circulant contains a regular abelian subgroup. Thus, such graphs are Cayley graphs.□

There are some vertex-transitive graphs, however, with automorphism groups which do not contain a regular subgroup. The Petersen graph shown in figure 2 is one such graph.

The automorphism group of this graph does contain a 10-element, transitive subset, however, which is very similar to a subgroup in structure. This subset is $M = \{\alpha^i \gamma^j \mid 0 \leqslant i < 2 \text{ and } 0 \leqslant j < 5\}$ where $\alpha = (1\ 6)\ (2\ 8\ 5\ 9)\ (3\ 10\ 4\ 7)$ and $\gamma = (1\ 2\ 3\ 4\ 5)\ (6\ 7\ 8\ 9\ 10)$. Note that M is not a subgroup as $\alpha^2 = (1)\ (6)\ (2\ 5)\ (3\ 4)\ (7\ 10)\ (8\ 9) \notin M$. Define $X_{M,e}$ to be the subgraph of the

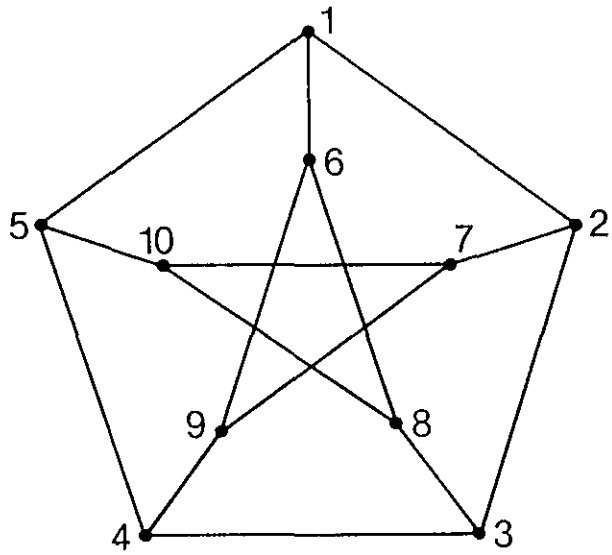

Figure 2

Petersen graph with ten nodes and edge set $\{\sigma(e)|\sigma\in M\}$ for any edge e. The subgraph $X_{M,e}$ is quite similar in structure to an orbit subgraph. In fact, it is not difficult to show that the $X_{M,e}$ satisfy the conditions stated in Lemmas 1–3. Since M has $o(V(X))=10$ elements, we may then apply the arguments of Theorem 2 to conclude that the Petersen graph may be expressed as the edge-disjoint union of multicycles. We now generalize this result.

DEFINITION: Given a graph X, a subset M of $G(X)$ is *grouplike* if for every edge $e\in E(X)$, the following three conditions are met:

GL1) $\forall\sigma_1\in M,\exists\sigma_2\in M$ such that $\sigma_2(e)=\sigma_1^{-1}(e)$,

GL2) $\forall\sigma_1,\sigma_2\in M,\exists\sigma_3\in M$ such that $\sigma_3(e)=\sigma_1\sigma_2(e)$, and

GL3) $\exists\sigma\in$M such that $\sigma(e)=e$.

Note that the definition of grouplike is very similar to that of a subgroup. The only difference is that we have reversed the order of the $\forall e$ and $\exists\sigma$ quantifiers in forming the definition of grouplike. Thus any subgroup of $G(X)$ is grouplike but not conversely. As an example, it is easily checked that $M=\{\alpha^i\gamma^j|0\leqslant i<2$ and $0\leqslant j<5\}$ is a grouplike subset, but not subgroup, of the automorphism group of the Petersen graph.

Let X be a graph, M a grouplike subset of $G(X)$ and e an edge in X. Define $X_{M,e}$ to be the subgraph of X with nodes $V(X)$ and edges $\{\sigma(e)|\sigma\in M\}$. The following are generalizations of Lemmas 1–3.

LEMMA 5: $X_{M,e}$ *is edge-transitive.*

PROOF: Given any $e_1,e_2\in E(X_{M,e})$, we know from the definition that $\exists\sigma_1,\sigma_2\in M$ such that $\sigma_1(e)=e_1$ and $\sigma_2(e)=e_2$. By GL1, we know that $\exists\sigma_3\in M$ such that $\sigma_3(e_1)=\sigma_1^{-1}(e_1)=e$. By GL2, we have that $\exists\sigma_4\in M$ such that $\sigma_4(e_1)=\sigma_2\sigma_3(e_1)=\sigma_2(e)=e_2$. Thus $X_{M,e}$ is edge-transitive.□

LEMMA 6: $M\subseteq G(X_{M,e})$.

PROOF: Given any $e\in E(X)$, $\sigma_1\in M$, and $e'\in E(X_{M,e})$, it suffices to show that $\sigma_1(e')\in E(X_{M,e})$. For then it will be clear that σ_1 preserves the edge structure of $X_{M,e}$ and thus that $\sigma_1\in G(X_{M,e})$ and that $M\subseteq G(X_{M,e})$. By definition, $\exists\sigma_2\in M$ such that $\sigma_2(e)=e'$. By GL2, $\exists\sigma_3\in M$ such that $\sigma_3(e)=\sigma_1\sigma_2(e)=\sigma_1(e')$. Thus $\sigma_1(e')\in E(X_{M,e})$ as desired.□

LEMMA 7: X *can be expressed as the edge-disjoint union of the distinct* $X_{M,e}$.

PROOF: We first show that for any $e_1,e_2\in E(X)$, either $E(X_{M,e_1})=E(X_{M,e_2})$ or $E(X_{M,e_1})\cap E(X_{M,e_2})=\emptyset$. In particular, choose $e\in E(X_{M,e_1})\cap E(X_{M,e_2})$. From the definition, we know that $\exists\sigma_1\in M$ such that $\sigma_1(e_1)=e$. By the transitivity of X_{M,e_2}, we know that given any $e_3\in E(X_{M,e_2})$, $\exists\sigma_2\in M$ such that $\sigma_2(e)=e_3$. Again applying GL2, this means that $\exists\sigma_3\in M$ such that $\sigma_3(e_1)=$

$\sigma_2\sigma_1(e_1)=\sigma_2(e)=e_3$. Thus $E(X_{M,e_2})\subseteq E(X_{M,e_1})$. By reversing e_1 and e_2 in the above argument, it is equally simple to show that $E(X_{M,e_1})\subseteq E(X_{M,e_2})$. Thus either $E(X_{M,e_1})\cap E(X_{M,e_2})=\emptyset$ or $E(X_{M,e_1})=E(X_{M,e_2})$.

The argument is completed by observing that every edge of X is included in some $X_{M,e}$ by GL3.□

We now state the corresponding generalization of Theorem 2.

THEOREM 3: *If the automorphism group of a vertex-transitive graph* X *contains an* o(V(X))*-element transitive grouplike subset, then* X *can be expressed as the edge-disjoint union of multicycles.*

PROOF: The proof is nearly identical to that of Theorem 2 and follows trivially from Lemmas 5–7.□

As we have been unable to find a vertex-transitive graph with an automorphism group which does not contain an $o(V(X))$-element transitive grouplike subset, we make the following conjecture.

CONJECTURE: *Every vertex-transitive graph can be expressed as the edge-disjoint union of multicycles.*

In Theorem 2, we verified the conjecture for all Cayley graphs, multidimensional circulants, and, in particular, for all vertex-transitive graphs with a prime number of nodes. Using a different approach, we now verify the conjecture in another case, one which has received attention recently [2,8,10].

THEOREM 4: *Every vertex-transitive graph with twice a prime number of nodes can be expressed as the edge-disjoint union of multicycles.*

PROOF: Let X be a vertex-transitive graph with $2p$ nodes where p is a prime. Since X is vertex-transitive, the subgroup of automorphisms of X which fix a given node has index $2p$ in $G(X)$. Thus $2p\,|\,o(G(X))$ and, by Sylow's Theorem, $G(X)$ contains an element γ of order p. Since $o(\gamma)=p$, γ is either the composition of two p-cycles or the composition of one p-cycle and p fixed elements. Label the nodes of X so that $V(X)=\{v_{i,j}\,|\,0\leqslant i<2 \text{ and } 0\leqslant j<p\}$ and $\gamma=(v_{0,0}\ldots v_{0,p-1})(v_{1,0}\ldots v_{1,p-1})$ or $\gamma=(v_{0,0}\ldots v_{0,p-1})(v_{1,0})\ldots(v_{1,p-1})$, depending on the structure of γ. We consider the two cases separately.

CASE 1: $\gamma=(v_{0,0}\ldots v_{0,p-1})(v_{1,0})\ldots(v_{1,p-1})$.

Without loss of generality, we can assume that $(v_{0,0},v_{1,0})\in E(X)$. Otherwise, X is disconnected and consists of two isomorphic, node-disjoint vertex-transitive graphs on p nodes each. Thus X is a multidimensional circulant and, by Corollary 1, is the edge-disjoint union of multicycles.

Since $\gamma\in G(X)$ and $(v_{0,0},v_{1,0})\in E(X)$, we know that $\gamma^j(v_{0,0},v_{1,0})=(v_{0,j},v_{1,0})\in E(X)$, for $0\leqslant j<p$ and thus $\deg(v_{1,0})\geqslant p$. Since X is vertex-transitive, it must be a regular graph and we know that $\deg(v_{1,j})\geqslant p$ for $0\leqslant j<p$. Thus for any j such that $0\leqslant j<p$, there exists an i such that $(v_{0,i},v_{1,j})\in E(X)$. Again applying the knowledge that $\gamma\in G(X)$, we find that $(v_{0,i},v_{1,j})\in E(X)$ for $0\leqslant i,j<p$. Thus X^c, the complement graph of X, is disconnected and, therefore, a multidimensional circulant. In [7], we show that X is a multidimensional circulant if and only if $G(X)$ contains a regular abelian subgroup. Since $G(X)=G(X^c)$, we conclude that X is also a multidimensional circulant.

CASE 2: $\gamma=(v_{0,0}\ldots v_{0,p-1})(v_{1,0}\ldots v_{1,p-1})$.

Define $V_i=\{v_{i,j}\,|\,0\leqslant j<p\}$ for $0\leqslant i<2$. Let E' be the set of edges of X with one endpoint in V_0 and one endpoint in V_1. Partition E' according to the congruence relation $e_1\sim e_2$ if $e_1=\gamma^j(e_2)$ for some j. Since γ is cyclic over V_0 and V_1, each block of the partition corresponds to p node-disjoint edges (i.e., a $C_{p,2}$ multicycle).

Now consider the edges E_i with both endpoints in V_i for $0\leqslant i<2$. In a similar fashion, partition E_0 and E_1. Each block of this partition corresponds to a p-cycle. Since X is vertex-transitive, it is regular. We already know that each vertex of X is incident to the same number of edges from E'. Thus $o(E_0)=o(E_1)$ and we can pair up p-cycles in E_0 with p-cycles in E_1 to form $C_{2,p}$ multicycles.

Summarizing, if X has at least one edge, then X is decomposable into $C_{p,2}$ multicycles, $C_{2,p}$ multicycles, or both. If $E(X)=\emptyset$, then $X\simeq C_{2p,1}$.□

4. Related Problems

We now consider the question of what multicycle decompositions a vertex-transitive graph can have. The graph in figure 3, for example, has three different multicycle decompositions.

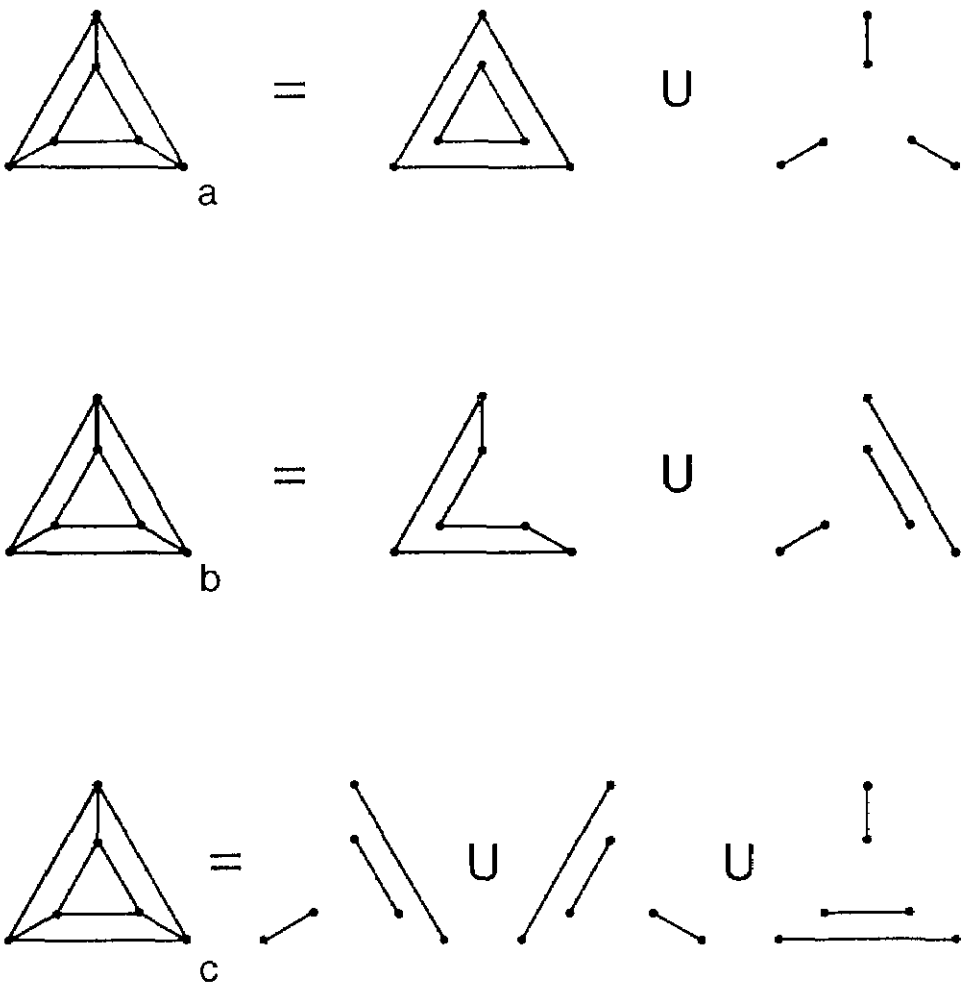

Figure 3

Define a *decomposition vector* **d** of a graph to be the vector $(d_1, \ldots, d_n)$ where $d_1, \ldots, d_n$ are such that X can be expressed as the edge-disjoint union of d_1 $C_{n,1}$ multicycles, d_2 $C_{n/2,2}$ multicycles, ..., and d_n $C_{1,n}$ multicycles. By convention, we set $d_1=0$ unless X has no edges, in which case $d_1=1$. We further require that $d_i=0$ for any i which does not integrally divide $n=o(V(X))$. As an example, we observe that the graph displayed in figure 3 has decomposition vectors (0,1,1,0,0,0), (0,1,0,0,0,1), and (0,3,0,0,0,0).

In the new terminology, the problem is to determine in some general way which decomposition vectors a given vertex-transitive graph can have. We now provide a partial solution to this problem.

THEOREM 5: *Let* X *be a multidimensional circulant with k-symbol* (**a**,S). *For each* $\mathbf{s}=(s_1, \ldots, s_k)\in S$, *define* $\rho(\mathbf{s})=\mathrm{lcm}(\frac{a_1}{\gcd(a_1,s_1)}, \ldots, \frac{a_k}{\gcd(a_k,s_k)})$. *Let* d_i *be the number of distinct unordered pairs* $\{\mathbf{s}, \mathrm{mod}(-\mathbf{s},\mathbf{a})\}$ *such that* $\mathbf{s}\in S$ *and* $\rho(\mathbf{s})=i$ *for* $1\leqslant i\leqslant n$. *If* X *has no edges, then define* $d_1=1$. *Then* $\mathbf{d}=(d_1, \ldots, d_n)$ *is a decomposition vector for* X.

PROOF: Let X be a multidimensional circulant with k-symbol $(\mathbf{a},S)$. We know from the definition of a multidimensional circulant that $E(X)=\{(v_i,v_j)\,|\,\mathrm{mod}(\mathbf{i-j,a})\in S\}$. For each $\mathbf{s}\in S$, define the subgraph $X_\mathbf{s}$ of X to be the graph with nodes $V(X)$ and edges $\{(v_i,v_j)\,|\,\mathrm{mod}(\mathbf{i-j,a})\in\{\mathbf{s},\mathrm{mod}(-\mathbf{s},\mathbf{a})\}\}$. It is clear that $X_\mathbf{s}=X_\mathbf{t}$ if and only if $\{\mathbf{s},\mathrm{mod}(-\mathbf{s},\mathbf{a})\}=\{\mathbf{t},\mathrm{mod}(-\mathbf{t},\mathbf{a})\}$. If $X_\mathbf{s}\neq X_\mathbf{t}$, then it is also clear that $E(X_\mathbf{s})\cap E(X_\mathbf{t})=\emptyset$. Thus X can be expressed as the edge-disjoint union of the $X_\mathbf{s}$.

We now complete the proof by showing that $X_\mathbf{s}\simeq C_{n/\rho(\mathbf{s}),\rho(\mathbf{s})}$ for all $\mathbf{s}\in S$ where $n=o(V(X))$. By definition, $X_\mathbf{s}$ is a vertex-transitive graph with k-symbol $(\mathbf{a},\{\mathbf{s},\mathrm{mod}(-\mathbf{s},\mathbf{a})\})$. Since $o(\{\mathbf{s},\mathrm{mod}(-\mathbf{s},\mathbf{a})\})\leqslant 2$, every node of $X_\mathbf{s}$ is adjacent to at most two other nodes. By Lemma 4, we know that $X_\mathbf{s}$ is a multicycle. From the definition of $E(X_\mathbf{s})$, we know that the length of each cycle in $X_\mathbf{s}$ is the smallest positive integer r such that $\mathrm{mod}(r\mathbf{s},\mathbf{a})=\mathbf{0}$. Note that $\mathrm{mod}(r\mathbf{s},\mathbf{a})=\mathbf{0}$ if and only if $a_i\,|\,rs_i$ for $1\leqslant i\leqslant k$ and thus if and only if $\frac{a_i}{gcd(a_i,s_i)}\,|\,r$ for $1\leqslant i\leqslant k$. Thus $\rho(s)=\mathrm{lcm}\,(\frac{a_1}{gcd(a_1,s_1)},\ \ldots\ ,\frac{a_k}{gcd(a_k,s_k)})$ is the smallest positive integer r such that $\mathrm{mod}(r\mathbf{s},\mathbf{a})=0$ and $X_\mathbf{s}\simeq C_{n/\rho(\mathbf{s}),\rho(\mathbf{s})}$.□

Note, however, that some multidimensional circulants may have multicycle decompositions not of the form specified in Theorem 5. For example, the decompositions in figures 3b and 3c do not correspond in any obvious way to the grouplike subsets of the automorphism group of the graph. Thus the complete determination of which decomposition vectors a vertex-transitive graph can have may well be a difficult problem.

Also of interest is the problem of how multicycles can be composed to form a vertex-transitive graph. Not every graph which can be expressed as the edge-disjoint union of multicycles is vertex-transitive. For instance, consider the graph shown in figure 4. This graph can be expressed as the edge-disjoint union of two 7-cycles, yet is not vertex-transitive. This fact is easily seen by observing that the complement of the graph is the node disjoint union of a 4-cycle and a 3-cycle and thus is not vertex-transitive.

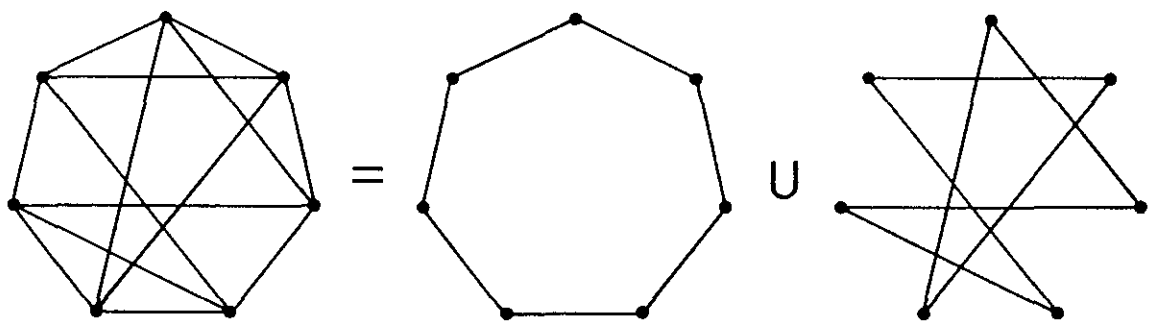

Figure 4

Thus the manner in which one can combine multicycles to form a vertex-transitive graph is not clear. A solution to the problem might well prove useful in settling the conjecture and in the development of a combinatorial characterization of the class of all vertex-transitive graphs.

In addition to Professor Maurer, the author would like to thank Professors Brian Alspach and Alan Goldman for their helpful remarks.

5. References

[1] Alspach B. Point-symmetric graphs and digraphs of prime order and transitive permutation groups of prime degree. J. Comb. Th. (B). **15**: 12–17; 1973.

[2] Alspach B.; Sutcliffe, R. J. Vertex-transitive graphs of order $2p$. submitted.

[3] Berggren, J. L. An algebraic characterization of symmetric graphs with p points, p an odd prime. Bull. Austral. Math Soc. 7: 131–134; 1972.
[4] Biggs, N. *Algebraic Graph Theory*. Great Britain: Cambridge University Press; 1974.
[5] Chao, C. On the classification of symmetric graphs with a prime number of vertices. Trans. Am. Math. Soc. **158**: 247–256; 1971.
[6] Folkman, J. Regular line-symmetric graphs. J. Comb. Th. 3; 215–232; 1967.
[7] Leighton, F. T. Circulants and the characterization of vertex-transitive graphs. J. Res. Natl. Bur. Stand. (U.S.). **88**(6); 395–402; 1983 November–December.
[8] Leighton, F. T. The characterization of vertex-transitive graphs. Senior thesis, Mathematics Department, Princeton University, unpublished; 1978.
[9] Sabidussi, G. Vertex-transitive graphs. Monatsh. Math. **68**: 426–438; 1964.
[10] Sutcliffe, R. J. Vertex-transitive graphs. M.Sc. thesis, Simon Fraser University, unpublished; 1974.
[11] Turner, J. Point-symmetric graphs with a prime number of points. J. Comb. Th. 3: 136–145; 1967.

JOURNAL OF RESEARCH of the National Bureau of Standards
Vol. 88, Nos. 1-6, January-December 1983

INDEX TO VOLUME 88

January-December 1983

Page

A

B

C

D

E

F

G

H

I

J

K

L

M

N

O

P–Q

R

S

T

U–V

W–Z